
ReLU to the Rescue: Improve Your On-Policy Actor-Critic with Positive Advantages

Andrew Jesson^{*1} Chris Lu² Gunshi Gupta¹
Angelos Filos¹ Jakob N. Foerster² Yarin Gal¹
¹OATML, University of Oxford ²FLAIR, University of Oxford

Abstract

In this paper, we introduce a novel method for enhancing the effectiveness of on-policy Deep Reinforcement Learning (DRL) algorithms. Current on-policy algorithms, such as Proximal Policy Optimization (PPO) and Asynchronous Advantage Actor-Critic (A3C), do not sufficiently account for cautious interaction with the environment. Our method addresses this gap by explicitly integrating cautious interaction in two critical ways: by maximizing a lower-bound on the true value function plus a constant, thereby promoting a *conservative value estimation*, and by incorporating Thompson sampling for cautious exploration. These features are realized through three surprisingly simple modifications to the A3C algorithm: (1) processing advantage estimates through a ReLU function, (2) spectral normalization, and (3) dropout. We provide theoretical proof that our algorithm maximizes the lower bound, which also grounds Regret Matching Policy Gradients (RMPG), a discrete-action on-policy method for multi-agent reinforcement learning. Our rigorous empirical evaluations across various benchmarks consistently demonstrates our approach's improved performance against existing on-policy algorithms. This research represents a substantial step towards more cautious and effective DRL algorithms, which has the potential to unlock application to complex, real-world problems.

1 Introduction

Deep Reinforcement Learning (DRL) is a paradigm to approximate solutions to complex sequential decision-making problems in domains such as robotics [Ibarz et al., 2021], autonomous driving [Kiran et al., 2021], strategy games [Mnih et al., 2015, Silver et al., 2017, Arulkumaran et al., 2019], and human computer interaction [Ziegler et al., 2019]. In recent years, DRL algorithms have achieved state-of-the-art performance on a variety of challenging benchmarks [Young and Tian, 2019, Lange, 2022, Todorov et al., 2012, Brockman et al., 2016]. However, their success in real-world applications does not only depend on their capacity to execute tasks while simultaneously refining the equations defining their action policy. It also hinges on a capacity for cautious policy execution in the face of finite observations of an ever changing world in order to avoid catastrophic results.

On-policy algorithms, such as Proximal Policy Optimization (PPO) [Schulman et al., 2017] or Asynchronous Advantage Actor-Critic (A3C) [Mnih et al., 2016], incorporate differentiable policies that are continuously updated based on recent interactions with the environment. Such recency bias, coupled with their potential to actively sample informative observations, makes on-policy approaches interesting candidates for applications in real-world non-stationary environments. However, neither PPO nor A3C explicitly account for cautious environmental interaction. In response, we propose a novel method that explicitly incorporates cautious decision-making in two significant ways: first, by

^{*}Correspondence to andrew.jesson@cs.ox.ac.uk. Implementation available at: <https://github.com/anndvision/vsop>

maximizing a lower-bound on the true value function plus a constant to promote algorithmic decision-making under a conservative estimate of value [Kumar et al., 2020]; and second, by integrating prudent exploration around action values with higher estimated value via Thompson sampling [Thompson, 1933]. This method is achieved through three surprisingly simple modifications to the A3C algorithm: first, the lower-bound on value is realized by processing advantage estimates through a ReLU function; second, the additive constant is regularized by applying spectral normalization to promote conservative estimates of value; and third, Thompson sampling is enabled by adopting dropout and weight normalization.

Through our thorough empirical assessments on the Gymnasium and Brax Mujoco benchmarks for continuous control [Brockman et al., 2016, Freeman et al., 2021], we show that our approach consistently outperforms existing on-policy algorithms such as PPO and A3C. Furthermore, our method shows competitive performance to these state-of-the-art on-policy methods in environments found in the MinAtar and ClassicControl benchmarks [Lange, 2022, Young and Tian, 2019]. Consequently, this paper offers a novel enhancement to boost the efficacy of on-policy DRL algorithms, underpinned by a comprehensive theoretical proof and extensive empirical evidence of its effectiveness. We believe that we are still far from algorithmic interaction with the world that is sufficiently cautious, but it is our hope that this research will catalyze the development of further cautious and effective applications of DRL for solving complex, real-world problems.

2 Background

Notation. We consider a discounted, T-horizon Markov Decision Process (MDP) defined by the tuple $(\mathcal{S}, \mathcal{A}, P, r, \gamma)$, where \mathcal{S} is the state space, \mathcal{A} is the action space, P is the state transition probability, r is the immediate reward upon transitioning from state s to state s' , and $\gamma \in [0, 1]$ is the discount factor. MDPs provide a framework for modeling sequential decision-making problems, where an agent interacts with an environment over discrete time steps to achieve a goal [Puterman, 2014]. Following the notation of Sutton and Barto [2018], we define states at time $t \in T$ by the d -dimensional, real-valued, random variable, $\mathbf{S}_t : \Omega \rightarrow \mathcal{S} \subseteq \mathbb{R}^d$, with observable instances $s_t = \mathbf{S}_t(\omega_t) : \forall \omega_t \in \Omega$. We define actions by the m -dimensional random variable $\mathbf{A}_t : \Omega \rightarrow \mathcal{A}$, with observable instances, $\mathbf{a}_t = \mathbf{A}_t(\omega_t) : \forall \omega_t \in \Omega$. Rewards are defined by the continuous-valued random variable, $R_t : \Omega \rightarrow \mathcal{R} \subseteq \mathbb{R}$, with observable instances, $r_t = R_t(\omega_t) : \forall \omega_t \in \Omega$. Let the random variable, $G_t := \sum_{k=t+1}^T \gamma^{k-1-t} R_k$, denote the discounted return. We use the standard definitions for the conditional action distribution/density (policy), $\pi(\mathbf{a} | \mathbf{s})$, the state value function under the policy, $v_\pi(\mathbf{s}) := \mathbb{E}_\pi [G_t | \mathbf{S}_t = \mathbf{s}]$, and state-action value function under the policy, $q_\pi(\mathbf{s}, \mathbf{a}) := \mathbb{E}_\pi [G_t | \mathbf{S}_t = \mathbf{s}, \mathbf{A}_t = \mathbf{a}]$.

On-policy, Actor-critic reinforcement learning. On-policy, Actor-critic approaches to reinforcement learning are called *policy-gradient* methods, in that they seek to optimize a differentiable, policy function, $\pi(\mathbf{a} | \mathbf{s}, \boldsymbol{\theta})$, with respect to the parameters, $\boldsymbol{\theta}$, in order to maximize the expected discounted return under the policy, $v_\pi(\mathbf{s})$. On-policy approaches differ from off-policy approaches in that they only use recent observations from the current policy to achieve this objective. Actor-critic methods differ from other policy-gradient methods because they fit an approximate value function (critic), $v(\mathbf{s}, \mathbf{w})$, to the data collected under the policy, in addition to optimizing the policy function (actor). The critic may be used in optimization of the actor, but is not generally used for decision making.

Deep reinforcement learning implements the actor and critic using neural network architectures, where the function parameters correspond to the weights of the networks. We denote the parameters of the actor and critic networks as $\boldsymbol{\theta}$ and \mathbf{w} , respectively. The output likelihood of the actor network is modeled using some distributional assumption informed by the nature of the action space, \mathcal{A} . For continuous action spaces, the likelihood is commonly modeled by an independent multivariate normal distribution with homogeneous noise variance, $\pi(\mathbf{a}_t | \mathbf{s}_t, \boldsymbol{\theta}) \sim \mathcal{N}(\mathbf{a} | \boldsymbol{\mu}(\mathbf{s}, \boldsymbol{\theta}), \mathbf{I}\sigma^2(\boldsymbol{\theta}))$, where $\sigma^2(\boldsymbol{\theta}) = (\sigma_1^2, \dots, \sigma_m^2)$ is the vector of inferred action noise variances. For discrete action spaces, the likelihood is generally modeled by a categorical distribution, $\pi(\mathbf{a}_t | \mathbf{s}_t, \boldsymbol{\theta}) \sim \text{Categorical}(\mathbf{a} | \boldsymbol{\mu}(\mathbf{s}, \boldsymbol{\theta}))$. In both cases, the mean parameter of the likelihood, $\boldsymbol{\mu}(\mathbf{s}, \boldsymbol{\theta})$, is the m -dimensional, vector-valued output of a neural network architecture with parameters, $\boldsymbol{\theta}$. Critic networks commonly fit using a mean squared error objective. This corresponds to an output likelihood modeled by a univariate normal distribution with unit variance, $p(g | \mathbf{s}, \mathbf{w}) \sim \mathcal{N}(g | v(\mathbf{s}, \mathbf{w}), 1)$, where the mean parameter is the approximate value function, $v(\mathbf{s}, \mathbf{w})$, and is given by the scalar-valued output of a neural network architecture with parameters, \mathbf{w} .

The baseline on-policy, actor-critic policy gradient algorithm seeks to perform gradient ascent with respect to the “performance” function, $J(\boldsymbol{\theta}) := v_\pi(\mathbf{s}_0, \boldsymbol{\theta})$, where $v_\pi(\mathbf{s}_0, \boldsymbol{\theta})$ is the true value function with respect to the parameters $\boldsymbol{\theta}$. By the policy gradient theorem [Sutton et al., 1999], we have: $\nabla_{\boldsymbol{\theta}} J(\boldsymbol{\theta}) = \nabla_{\boldsymbol{\theta}} v_\pi(\mathbf{s}_0) \propto \int_{\mathcal{S}} \rho(\mathbf{s}) \int_{\mathcal{A}} q_\pi(\mathbf{s}, \mathbf{a}) \nabla_{\boldsymbol{\theta}} \pi(\mathbf{a} | \mathbf{s}, \boldsymbol{\theta}) d\mathbf{a} ds$. Sutton and Barto [2018] show that a generalization of this result includes a comparison of the state-action value function, $q_\pi(\mathbf{s}, \mathbf{a})$, to an arbitrary baseline that does not vary with the action, \mathbf{a} . When the baseline is chosen to be the state value function, $v_\pi(\mathbf{s})$, we have an objective in terms of the *advantage function* [Schulman et al., 2015b], $h_\pi(\mathbf{s}, \mathbf{a}) := q_\pi(\mathbf{s}, \mathbf{a}) - v_\pi(\mathbf{s})$, namely: $\nabla_{\boldsymbol{\theta}} J(\boldsymbol{\theta}) \propto \int_{\mathcal{S}} \rho(\mathbf{s}) \int_{\mathcal{A}} h_\pi(\mathbf{s}, \mathbf{a}) \nabla_{\boldsymbol{\theta}} \pi(\mathbf{a} | \mathbf{s}, \boldsymbol{\theta}) d\mathbf{a} ds$. This *all actions* formulation can be further simplified in terms of observed actions and states as: $\nabla_{\boldsymbol{\theta}} J(\boldsymbol{\theta}) \propto \mathbb{E}_\pi [h_\pi(\mathbf{S}_t, \mathbf{A}_t) \nabla_{\boldsymbol{\theta}} \log \pi(\mathbf{A}_t | \mathbf{S}_t, \boldsymbol{\theta})]$. We use \mathbb{E}_π to denote an expectation over states \mathbf{S}_t and actions \mathbf{A}_t collected under the policy $\pi(\mathbf{a} | \mathbf{s})$.

In general, because neither the state-action, $q_\pi(\mathbf{s}, \mathbf{a})$, nor the state value, $v_\pi(\mathbf{s})$, functions are given, we need an estimator for the advantage function. For compactness, we will focus on the generalized advantage estimator (GAE) proposed by Schulman et al. [2015b]: $h(\mathbf{s}_t, \mathbf{r}_t, \mathbf{w}) = \sum_{k=t+1}^T (\gamma\lambda)^{k-1-t} \delta_{t-k+1}^{\mathbf{w}}$, where $0 < \lambda \leq 1$, and $\delta_t^{\mathbf{w}} = r_t + \gamma v(\mathbf{s}_{t+1}; \mathbf{w}) - v(\mathbf{s}_t; \mathbf{w})$ is the temporal difference (TD) residual of the value function with discount, γ [Sutton and Barto, 2018]. The GAE then yields a low-variance gradient estimator for the policy function: $\widehat{\nabla_{\boldsymbol{\theta}} J(\boldsymbol{\theta})} := \mathbb{E}_\pi [h(\mathbf{S}_t, \mathbf{R}_t, \mathbf{w}) \nabla_{\boldsymbol{\theta}} \log \pi(\mathbf{A}_t | \mathbf{S}_t, \boldsymbol{\theta})]$.

Finally, the actor and critic networks are generally optimized by using mini-batch stochastic gradient descent Robbins and Monro [1951] to fit the functions induced by the network weights to a batch of data collected under the current policy, $\mathcal{D}_\pi^b = \{\mathbf{s}_i, \mathbf{a}_i, r_i\}_{i=1}^b$.

3 Methods

In this section we develop our cautious, on-policy actor-critic algorithm. As a reminder, this algorithm is realized by making three simple changes to the A3C algorithm: first, advantage estimates are processed through a ReLU function; second, network weights are regularized using spectral normalization; and third, actor and critic networks are implemented as Bayesian Neural Networks to enable Thompson sampling. We provide the theoretical grounding to prove that clipping the advantages during policy optimization results in the optimization of a lower-bound on the true value function plus a constant. We show that under standard assumptions the constant is equal to is the expected, clipped difference in the state value function, $\gamma v_\pi(\mathbf{s}') - v_\pi(\mathbf{s})$, over all actions, \mathbf{a} , and next states, \mathbf{s}' , under the policy given state, \mathbf{s} , and that it can be regularized using spectral normalization. And finally, we detail how to enable cautious exploration via Thompson sampling using just dropout and weight decay. The following theorem formalizes the main result of our paper.

Theorem 3.1. *Let, $G_t := \sum_{k=t+1}^T \gamma^{k-1-t} R_k$, denote the discounted return. Let $q_\pi(\mathbf{s}, \mathbf{a}) = \mathbb{E}_\pi [G_t | \mathbf{S}_t = \mathbf{s}, \mathbf{A}_t = \mathbf{a}]$, denote the state-action value function, and $v_\pi(\mathbf{s}) = \mathbb{E}_\pi [G_t | \mathbf{S}_t = \mathbf{s}]$, denote the state value function, under policy $\pi(\mathbf{a} | \mathbf{s}, \boldsymbol{\theta})$. Let $(x)^+ := \max(0, x)$. Assume, without loss of generality, that rewards, R_t , are non-negative. Assume that the gradient of the policy, $\nabla_{\boldsymbol{\theta}} \pi(\mathbf{a} | \mathbf{s}, \boldsymbol{\theta})$, is a conservative vector field. Then, performing gradient ascent with respect to,*

$$\nabla_{\boldsymbol{\theta}} J(\boldsymbol{\theta}) = \mathbb{E}_\pi \left[\left(q_\pi(\mathbf{S}_t, \mathbf{A}_t) - v_\pi(\mathbf{S}_t) \right)^+ \nabla_{\boldsymbol{\theta}} \log \pi(\mathbf{A}_t | \mathbf{S}_t, \boldsymbol{\theta}) \right], \quad (1)$$

maximizes a lower-bound, $v_\pi^(\mathbf{s})$, on the state value function, $v_\pi(\mathbf{s})$, plus a constant:*

$$v_\pi^*(\mathbf{s}) \leq v_\pi(\mathbf{s}) + C(\mathbf{s}), \quad (2)$$

where, $C(\mathbf{s}) = \iint \left(\gamma v_\pi(\mathbf{s}') - v_\pi(\mathbf{s}) \right)^+ d\mathbb{P}(\mathbf{s}' | \mathbf{S}_t = \mathbf{s}, \mathbf{A}_t = \mathbf{a}) d\Pi(\mathbf{a} | \mathbf{S}_t = \mathbf{s})$, is the expected, clipped difference in the state value function, $\gamma v_\pi(\mathbf{s}') - v_\pi(\mathbf{s})$, over all actions, \mathbf{a} , and next states, \mathbf{s}' , under the policy given state, \mathbf{s} . Here, we use $\int \dots d\Pi(\mathbf{a} | \mathbf{s})$ to denote $\sum_{\mathbf{a}} \dots \pi(\mathbf{a} | \mathbf{s})$ for discrete action spaces and $\int \dots \pi(\mathbf{a} | \mathbf{s}) d\mathbf{a}$ for continuous action spaces. Similarly, we use $\int \dots d\mathbb{P}(\mathbf{s}' | \mathbf{s}, \mathbf{a})$ to denote $\sum_{\mathbf{s}'} \dots p(\mathbf{s}' | \mathbf{s}, \mathbf{a})$ for discrete state spaces and $\int \dots p(\mathbf{s}' | \mathbf{s}, \mathbf{a}) d\mathbf{s}'$ for continuous state spaces. Proof is provided in Appendix A.1.

Bounding the constant $C(\mathbf{s})$. Considering the value function, $v_\pi(\mathbf{s})$, as K -Lipschitz continuous and assuming that the expected value of the value function, $v_\pi(\mathbf{s}')$ over next states, \mathbf{s}' , is equal to

the value function evaluated at the current state, $v_\pi(\mathbf{s})$. Then, when $\gamma = 1$, the constant is bounded proportional to the expected absolute difference between states.

$$\begin{aligned}
C(\mathbf{s}) &= \iint \left(v_\pi(\mathbf{s}') - v_\pi(\mathbf{s}) \right)^+ d\mathbb{P}(\mathbf{s}' \mid \mathbf{S}_t = \mathbf{s}, \mathbf{A}_t = \mathbf{a}) d\Pi(\mathbf{a} \mid \mathbf{S}_t = \mathbf{s}) \\
&= \frac{1}{2} \iint \left(v_\pi(\mathbf{s}') - v_\pi(\mathbf{s}) + |v_\pi(\mathbf{s}') - v_\pi(\mathbf{s})| \right) d\mathbb{P}(\mathbf{s}' \mid \mathbf{S}_t = \mathbf{s}, \mathbf{A}_t = \mathbf{a}) d\Pi(\mathbf{a} \mid \mathbf{S}_t = \mathbf{s}) \\
&= \frac{1}{2} \iint |v_\pi(\mathbf{s}') - v_\pi(\mathbf{s})| d\mathbb{P}(\mathbf{s}' \mid \mathbf{S}_t = \mathbf{s}, \mathbf{A}_t = \mathbf{a}) d\Pi(\mathbf{a} \mid \mathbf{S}_t = \mathbf{s}) \\
&\leq \frac{1}{2} \iint K \|\mathbf{s}' - \mathbf{s}\| d\mathbb{P}(\mathbf{s}' \mid \mathbf{S}_t = \mathbf{s}, \mathbf{A}_t = \mathbf{a}) d\Pi(\mathbf{a} \mid \mathbf{S}_t = \mathbf{s}).
\end{aligned} \tag{3}$$

This interpretation motivates using spectral normalization [Miyato et al., 2018] of the value function estimator weights, $v(\mathbf{s}, \mathbf{w})$, which regulates the Lipschitz constant, K , of the estimator and has been shown to improve performance in the off-policy reinforcement learning setting [Bjorck et al., 2021, Gogianu et al., 2021]. Moreover, when using the generalized advantage estimator with the same assumptions, the constant is given by: $C(\mathbf{s}) = \frac{1}{2} \iint |\gamma \lambda v_\pi(\mathbf{s}') - v_\pi(\mathbf{s})| d\mathbb{P}(\mathbf{s}' \mid \mathbf{S}_t = \mathbf{s}, \mathbf{A}_t = \mathbf{a}) d\Pi(\mathbf{a} \mid \mathbf{S}_t = \mathbf{s})$. Since $\gamma \lambda < 1$, the GAE also serves to regularize the constant.

Cautious exploration. We propose doing Bayesian inference over the actor and critic parameters in order to enable cautious exploration via Thompson sampling [Thompson, 1933]. This involves introducing posterior distributions over the policy parameters, $q(\boldsymbol{\theta} \mid \mathcal{D}_{n-1})$, and value function estimator parameters, $q(\mathbf{W} \mid \mathcal{D}_{n-1})$. Here, $\mathcal{D}_{n-1} = \{\mathbf{s}_i, \mathbf{a}_i, r_i\}_{i=1}^{|\mathcal{T}_{n-1}|}$ is data collected under the policy, $\pi(\mathbf{a} \mid \mathbf{s}, \boldsymbol{\theta}_{n-1})$, over a set of horizons, $\mathcal{T}_{n-1} = \mathbb{T}_1^{n-1} \cup \mathbb{T}_2^{n-1} \cup \dots$. In general, any inference technique can be used. In Algorithm 1, we outline the procedure for the case of approximate inference using dropout Bayesian Neural Networks (BNNs) following Gal and Ghahramani [2016]. For a dropout BNN, the posterior distribution for the policy parameters is of the form $q(\boldsymbol{\theta} \mid \hat{\boldsymbol{\theta}}, p)$, where $\hat{\boldsymbol{\theta}}$ is the expected value of the parameters, and p is the dropout rate. Similarly, the posterior distribution for the value function parameters is of the form $q(\mathbf{w} \mid \hat{\mathbf{w}}, p)$, where $\hat{\mathbf{w}}$ is the expected value of the parameters, and p is the dropout rate. Each dropout BNN is optimized by minimizing the Kullback–Leibler divergence between a prior distribution and its approximate posterior.

We term this method VSOP, for Variational [b]ayes, Spectral-normalized, On-Policy reinforcement learning. Algorithm 1 details VSOP for dropout BNNs.

Algorithm 1 VSOP for Dropout Bayesian Neural Networks

Require: initial state, \mathbf{s}' , environment, $p(\mathbf{s}', r \mid \mathbf{s}, \mathbf{a})$, rollout buffer, \mathcal{D} , initial actor parameters, $\hat{\boldsymbol{\theta}}$, initial critic parameters, $\hat{\mathbf{w}}$, dropout rate, p , learning rate, η , minibatch size, b .

```

1: while true do
2:    $\mathcal{D} \leftarrow \emptyset$  ▷ reset rollout buffer
3:   while acting do ▷ interact with the environment
4:      $\mathbf{s} \leftarrow \mathbf{s}'$  ▷ update current state
5:      $\boldsymbol{\theta} \sim q(\boldsymbol{\theta} \mid \hat{\boldsymbol{\theta}}, p)$  if TS else  $\boldsymbol{\theta} \leftarrow \hat{\boldsymbol{\theta}}$  ▷ sample actor params if Thompson sampling (TS)
6:      $\mathbf{a} \sim \pi(\mathbf{a} \mid \mathbf{s}, \boldsymbol{\theta})$  ▷ sample action from policy
7:      $\mathbf{s}', r \sim p(\mathbf{s}', r \mid \mathbf{s}, \mathbf{a})$  ▷ sample next state and reward from environment
8:      $\mathcal{D} \leftarrow \mathcal{D} \cup \{(\mathbf{s}, \mathbf{a}, r)\}$  ▷ update rollout buffer
9:    $\mathbf{w}^* \leftarrow \hat{\mathbf{w}}$  ▷ freeze critic weights for advantage estimates
10:   $\beta \leftarrow (1 - p) / (2|\mathcal{D}|)$  ▷ set parameter precision
11:  while fitting do ▷ update actor and critic
12:     $\{\mathbf{s}_i, \mathbf{a}_i, r_i\}_{i=1}^b \sim \mathcal{D}$  ▷ sample minibatch from rollout buffer
13:     $\tilde{\mathbf{w}} \sim q(\mathbf{w} \mid \mathbf{w}^*, p)$  if TS else  $\tilde{\mathbf{w}} \leftarrow \mathbf{w}^*$  ▷ sample advantage params if TS
14:     $\boldsymbol{\theta} \sim q(\boldsymbol{\theta} \mid \hat{\boldsymbol{\theta}}, p)$  ▷ sample actor parameters
15:     $\hat{\boldsymbol{\theta}} \leftarrow \hat{\boldsymbol{\theta}} - \eta \frac{1}{b} \sum_{i=1}^b h^+(\mathbf{s}_i, r_i, \tilde{\mathbf{w}}) \nabla_{\boldsymbol{\theta}} \log \pi(\mathbf{a}_i \mid \mathbf{s}_i, \boldsymbol{\theta}) + 2\beta \boldsymbol{\theta}$  ▷ update actor
16:     $\mathbf{w} \sim q(\mathbf{w} \mid \hat{\mathbf{w}}, p)$  ▷ sample critic parameters
17:     $\hat{\mathbf{w}} \leftarrow \hat{\mathbf{w}} - \eta \frac{1}{b} \sum_{i=1}^b \nabla_{\mathbf{w}} \log p(g(\mathbf{s}_i, r_i, \tilde{\mathbf{w}}) \mid \mathbf{s}_i, \mathbf{w}) + 2\beta \mathbf{w}$  ▷ update critic

```

4 Related Works

4.1 On-policy methods

VSOP is an on-policy RL algorithm. Table 1 compares the gradient of the performance function, $\nabla J(\theta)$, for VSOP with those for relevant on-policy algorithms. We discuss each algorithm below

Table 1: Comparison of performance functions for on-policy methods

Method	$\nabla J(\theta)$
A3C	$\mathbb{E}_\pi [h_\pi(\mathbf{S}_t, \mathbf{A}_t) \nabla \log \pi(\mathbf{A}_t \mathbf{S}_t, \theta)]; \quad h_\pi(\mathbf{S}_t, \mathbf{A}_t) = q_\pi(\mathbf{S}_t, \mathbf{A}_t) - v_\pi(\mathbf{S}_t)$
VSOP	$\mathbb{E}_\pi [h_\pi^+(\mathbf{S}_t, \mathbf{A}_t) \nabla \log \pi(\mathbf{A}_t \mathbf{S}_t, \theta)]; \quad h_\pi^+(\mathbf{S}_t, \mathbf{A}_t) = \max(0, h_\pi(\mathbf{S}_t, \mathbf{A}_t))$
RMPG	$\mathbb{E}_\pi [\int h_\pi^+(\mathbf{S}_t, \mathbf{a}) \nabla d\Pi(\mathbf{a} \mathbf{S}_t, \theta)]$
TRPO	$\mathbb{E}_\pi [h_\pi(\mathbf{S}_t, \mathbf{A}_t) \nabla \rho(\mathbf{S}_t, \mathbf{A}_t, \theta)]; \quad \rho(\mathbf{S}_t, \mathbf{A}_t, \theta) = \frac{\pi(\mathbf{A}_t \mathbf{S}_t, \theta)}{\pi(\mathbf{A}_t \mathbf{S}_t, \theta_{\text{old}})}$
PPO	$\mathbb{E}_\pi \left[\min \left(h_\pi(\mathbf{S}_t, \mathbf{A}_t) \nabla \rho(\mathbf{S}_t, \mathbf{A}_t, \theta), \text{clip} \left(h_\pi(\mathbf{S}_t, \mathbf{A}_t) \nabla \rho(\mathbf{S}_t, \mathbf{A}_t, \theta), 1 - \epsilon, 1 + \epsilon \right) \right) \right]$
DPO	$\mathbb{E}_\pi \left[\nabla \begin{cases} (h_\pi(\rho(\theta) - 1) - a \tanh(h_\pi(\rho(\theta) - 1)/a))^+ & h_\pi(\mathbf{S}_t, \mathbf{A}_t) \geq 0 \\ (h_\pi \log(\rho(\theta)) - b \tanh(h_\pi \log(\rho(\theta))/b))^+ & h_\pi(\mathbf{S}_t, \mathbf{A}_t) < 0 \end{cases} \right]$
CVaR	$\mathbb{E}_\pi \left[(\nu_\alpha - G_t)^+ \nabla \log \pi(\mathbf{A}_t \mathbf{S}_t, \theta) \right]; \quad \nu_\alpha := \alpha\text{-quantile of return, } G_t$
RSPG	$\mathbb{E}_\pi \left[(G_t - \nu_\alpha)^+ \nabla \log \pi(\mathbf{A}_t \mathbf{S}_t, \theta) \right]; \quad G_t := \sum_{k=t+1}^T \gamma^{k-1-t} R_k$
EPOpt	$\mathbb{E}_\pi [\mathbb{1}(G_t \leq \nu_\alpha) \nabla J(\theta, \mathbf{S}_t, \mathbf{A}_t)]; \quad J(\theta, \mathbf{S}_t, \mathbf{A}_t)$ on-policy perf. function

4.1.1 Mirror Learning

Trust Region Policy Optimization (TRPO) [Schulman et al., 2015a] is an on-policy, actor-critic method that improves upon the baseline policy gradient method by incorporating a constraint on the maximum size of policy updates. TRPO takes small steps in the direction of improvement and limits the step size to ensure that the new policy does not deviate significantly from the old policy. This is achieved by optimizing a surrogate objective function that approximates the expected reward under the new policy while imposing a constraint on the KL divergence between the new and old policies. TRPO has been shown to be effective in various high-dimensional and continuous control tasks. **Proximal Policy Optimization (PPO)** [Schulman et al., 2017] is closely related to TRPO. Like TRPO, PPO improves upon the baseline policy gradient method by constraining the maximum size of policy updates. However, instead of using a KL divergence constraint, PPO employs a clipped surrogate objective function to limit the size of policy updates. PPO simplifies the optimization procedure compared to TRPO, making it more computationally efficient and easier to implement. While TRPO and PPO constrain policy updates based on the ratio between the new and old policies, VSOP constrains policy updates according to the sign of the estimated advantage function. Notably, PPO and TRPO are instances of the *mirror learning* framework Kuba et al. [2022], whereas VSOP does not inherit the same theoretical guarantees. Lu et al. [2022] explores the Mirror Learning space by meta-learning a “drift” function. They term their immediate result Learned Policy Optimization (LPO). Through its analysis they arrive at **Discovered Policy Optimisation (DPO)**, a novel, closed-form RL algorithm.

4.1.2 Regret Matching Policy Gradient (RMPG)

RMPG [Srinivasan et al., 2018] is inspired by an objective called regret policy gradient (RPG), which maximizes a lower-bound on the advantages: $(h(s, \mathbf{a}))^+ \leq h(s, \mathbf{a})$. RPG optimizes the policy directly with respect to an estimator of the advantage lower-bound, denoted as $\nabla_\theta J^{\text{RPG}}(\theta)$. RMPG, being inspired by RPG, has a different objective, $\nabla_\theta J^{\text{RMPG}}(\theta)$. In both cases, $q(s, \mathbf{a}, \mathbf{w})$ is a parametric estimator of the state-action value function, $q_\pi(s, \mathbf{a})$. RMPG has demonstrated improved sample efficiency and stability in learning compared to standard policy gradient methods. VSOP is closely related to RMPG; however, we provide the missing theoretical foundations to ground RMPG (Appendix A.1), extend RMPG from the *all actions* formulation making it more suitable for continuous control (Appendix A.2), and employ the GAE rather than the state-action value function estimator, $q(s, \mathbf{a}, \mathbf{w})$.

4.1.3 Risk Sensitive Reinforcement Learning.

Instead of optimizing expected value, risk sensitive RL methods optimize a measure of risk. Tamar et al. [2015] propose the risk averse **CVaR-PG** which seeks to minimize the Conditional Value at Risk (CVaR), $\Phi(\theta) := \mathbb{E}_\pi [G_t \mid G_t \leq \nu_\alpha]$, where ν_α is the α -quantile of the return, G_t , distribution under policy, $\pi(\mathbf{a} \mid \mathbf{s}, \theta)$. Relatedly, Tang et al. [2020] have used the CVaR as a baseline function for standard policy updates. By focusing only on the worse case trajectories, **CVaR-PG** is susceptible “blindness to success,” thus Greenberg et al. [2022] propose a Cross-entropy Soft-Risk algorithm (CeSoR) to address this. Kenton et al. [2019] and Filos et al. [2022] also propose uncertainty aware, risk-averse methods. In contrast to the above risk averse methods, Petersen et al. [2019] present **Risk Seeking Policy Gradient (RSPG)** which focuses on maximizing best-case performance by only performing gradient updates when rewards exceed a specified quantile of the reward distribution. Prashanth et al. [2022] provide a comprehensive discussion on risk-sensitive RL.

4.2 Off-policy methods

Self Imitation Learning (SIL) [Oh et al., 2018] is a hybrid method that uses clipped advantage estimates to improve the performance of on-policy algorithms such as PPO and A2C by learning from its own successful off-policy trajectories. By leveraging experience replay, SIL encourages the agent to imitate its own high-reward actions. **Self Imitation Advantage Learning (SIAL)** [Ferret et al., 2020] is an extension of SIL that incorporates an advantage function to guide the learning process. SIAL uses the clipped advantage function to weigh the importance of different actions during self-imitation, enabling the agent to focus on actions that yield higher long-term rewards. This approach leads to more efficient learning and improved performance in complex environments. Importantly, even though SIL and SIAL only update policies when advantage estimates are positive, they differ from VSOP in that they are off-policy algorithms that learn from successful past trajectories and they optimize different objectives based on max-entropy reinforcement learning [Aghasadeghi and Bretl, 2011, Haarnoja et al., 2018].

4.3 Thompson Sampling in Deep Reinforcement Learning

Thompson sampling has most frequently been explored in the context of Q-Learning [Strens, 2000, Wang et al., 2005] and Deep Q-Learning [Osband et al., 2016, Moerland et al., 2017, Azizzadenesheli et al., 2018] to improve exploration and sample efficiency. Related sampling-based exploration strategies for Deep Q-Learning have also been proposed by Clements et al. [2019], Nikolov et al. [2018].

In the context of policy gradient methods, related Upper confidence bound (UCB) [Ciosek et al., 2019] and Hamiltonian Monte-Carlo (HMC) [Xu and Fekri, 2022] approaches are proposed for off-policy Soft Actor-Critic (SAC) [Haarnoja et al., 2018], and Henaff et al. propose an elliptical episodic reward for general use. For model-based policy gradient methods, Rajeswaran et al. [2016] propose **Ensemble Policy Optimization (EPOpt)** which incorporates restricting policy updates to be risk-averse based on the CVaR and uses ensembles to sample hypothesized models. However, we believe our work is the first to show the benefit of Thompson sampling in the context of on-policy actor-critic methods.

5 Experiments

We conduct a comprehensive evaluation of VSOP against on-policy RL methods across various domains, with both continuous and discrete action spaces and diverse dimensionalities in both the action and observation spaces. Furthermore, we evaluate our method using both the PyTorch [Paszke et al., 2019] and JAX [Bradbury et al., 2018] frameworks. In Section 5.1, we compare VSOP to baseline implementations of PPO, A3C, and RMPG on the Gymnasium [Brockman et al., 2016] implementation of Mujoco [Todorov et al., 2012] for continuous control (Section 5.1.1). In this setting, we further ablate the effect that positive advantages, spectral normalization, and Thompson sampling each have on performance (Section 5.1.2), investigate the relationship between Thompson sampling and asynchronous parallelization (Appendix C.1), show that spectral normalization and Thompson sampling also have non-negligible positive effects for PPO (Appendix C.2), and offer comparison to off-policy approaches like SAC [Haarnoja et al., 2018] and Twin Delayed DDPG

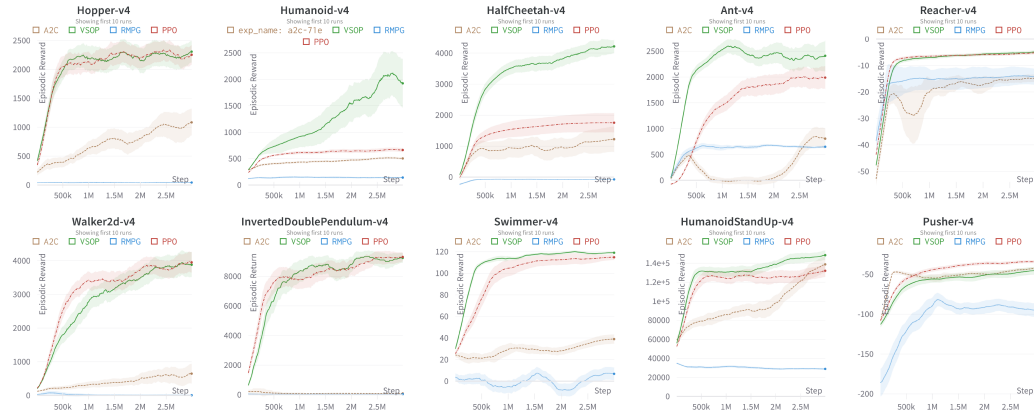


Figure 1: Gymnasium-Mujoco. Comparing VSOP to on-policy baseline algorithms. Here, VSOP improves over baseline PPO in 5 environments, matches it’s performance in 4 environments, and is worse in just 1 environment, Pusher. VSOP improves over A2C in all environments but Pusher, where performance is statistically equal. Finally, VSOP improves over RMPG in all environments.

(TD3) [Fujimoto et al., 2018] (Section 5.1.3). In Section 5.2, we exploit the fast iteration cycles offered by vectorized JAX implementations and the gymnasium framework [Lange, 2022] to perform fair comparisons of VSOP, PPO, and A2C when each have been given equal hyper-parameter search budgets.

5.1 Gymnasium Mujoco

For this evaluation we build off of Huang et al. [2022]’s CleanRL package which provides reproducible, user-friendly implementations of state-of-the-art reinforcement learning algorithms using PyTorch [Paszke et al., 2019], Gymnasium [Brockman et al., 2016, Todorov et al., 2012], and Weights & Biases [Biases, 2018]. Overall, we find that several of the code-level optimizations key to PPO reproducibility are superfluous for our method [Engstrom et al., 2020, Andrychowicz et al., 2021]. Particularly, we omit advantage normalization, value loss clipping [Schulman et al., 2017], gradient clipping, and modification of the default Adam [Kingma and Ba, 2014] epsilon parameter as they either do not lead to an appreciable difference in performance or have a slightly negative effect. However, we find that orthogonal weight initialization, learning rate annealing, reward scaling/clipping, and observation normalization/clipping remain having non-negligible positive effects on performance [Engstrom et al. 2020, Andrychowicz et al. 2021]. In addition to adding dropout, weight decay regularization, and spectral normalization, we also look at model architecture modifications not present in the CleanRL implementation: layer width, number of hidden layers, layer activation, layer normalization [Ba et al. 2016], and residual connections. We find that ReLU activation functions [Nair and Hinton, 2010], increasing layer width to 256, and a small dropout rate of 0.01-0.04 are beneficial. We find that network depth, and residual connections are benign overall. In contrast to recent findings in the context of offline data for off-policy reinforcement learning [Ball et al., 2023], we find that layer normalization — whether applied to the actor, the critic, or both — is detrimental to performance. Full details are given in Appendix B.1.

5.1.1 Comparison to on-policy baselines.

First we compare tuned VSOP to baseline implementations of PPO, A2C, and RMPG. We use the CleanRL [Huang et al., 2022] implementation of PPO, the StableBaselines3 [Raffin et al., 2021] hyper-parameter settings for A2C, and the VSOP optimal hyper-params for RMPG. Figure 1 summarizes these results. VSOP improves over baseline PPO in 5 environments, matches it’s performance in 4 environments, and is worse in just 1 environment, Pusher. VSOP improves over A2C in all environments but Pusher, where performance is statistically equal. Finally, VSOP improves over RMPG in all environments.

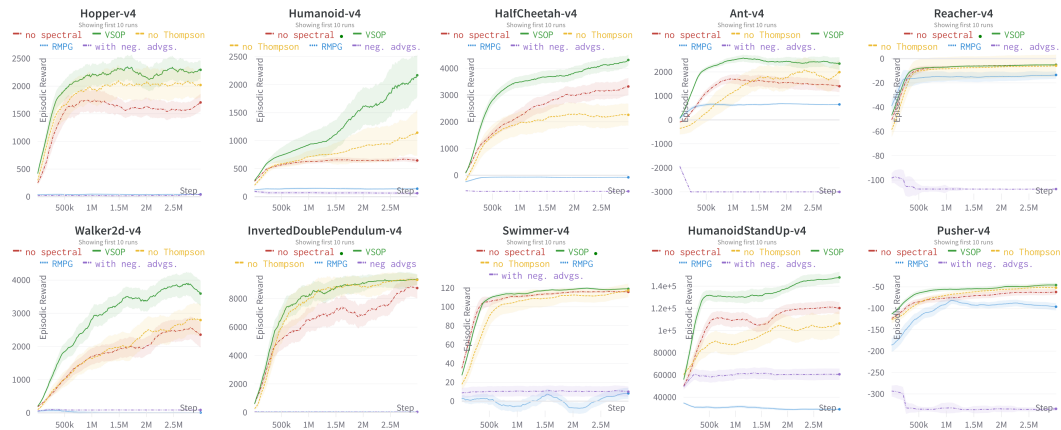


Figure 2: Comparing the effect of VSOP mechanisms on Mujoco continuous control performance. We see that using the single action framework and updating the policy only when the estimated advantages are positive have the largest effects, followed by spectral normalization, and finally Thompson sampling. Green solid lines (VSOP) show proposed, optimized method. Yellow dashed lines (no Thomp. samp.) show VSOP less Thompson sampling when acting or estimating advantages. Red dash dot lines (no spect. norm.) show VSOP less spectral normalization. Blue dotted lines (RMPG) show the “all actions” approach. Purple dash dot dot lines (with neg. advantages) show VSOP without restricting policy updates to positive advantages.

5.1.2 Ablation of mechanisms.

Next, we investigate the influence of our four proposed mechanisms on the performance of VSOP. As a reminder, the mechanisms are positive-advantages, single-action setting, spectral normalization, and Thompson sampling. Figure 2 summarizes these results. We see that positive advantages and operating in the single-action regime have the largest influences on performance. Spectral normalization and Thompson sampling also have large influences, especially in high-dimensional action and observation space settings such as Humanoid, Humanoid Stand-Up, and Ant. The performance gains for spectral normalization are aligned with results given by Bjorck et al. [2021] and Gogianu et al. [2021] for DDPG [Lillicrap et al., 2015], DRQ [Kostrikov et al., 2020], Dreamer [Hafner et al., 2019], DQN [Wang et al., 2016] and C51 [Bellemare et al., 2017].

5.1.3 Closing the gap to off-policy methods

Interestingly, we see that applying spectral normalization and dropout to PPO also yields an improvement. We call this augmentation VSPPO and provide detailed analysis in Appendix C.2. In Figure 3, we compare VSOP and VSPPO to SAC and TD3, and see that we close the performance gap significantly for environments such as Humanoid, Half-Cheetah, Ant, and Humanoid Stand-up.

5.2 Gymnax Environments

Gymnax [Lange, 2022] and Jax [Bradbury et al., 2018] facilitate vectorization enabling principled hyper-parameter tuning by building off of PureJaxRL [Lu et al., 2022]. Here we explore several environments and compare VSOP, PPO, and A3C. We use Bayesian hyper-parameter optimization [Snoek et al., 2012] and give each algorithm a search budget of 100 steps. The search space is comprised of the learning rate, learning rate annealing, number of update epochs, number of minibatches in an update epoch, the GAE λ parameter, the max gradient norm, the width of the network, and the steps to environments ratio for a fixed number of steps between updates. Full implementation details are given in Appendix B.2. **Brax Mujoco.** Figure 5 summarize the results for Brax Mujoco [Todorov et al., 2012, Freeman et al., 2021]. We see that VSOP beats PPO on 5 of the 9 environments, and that VSOP beats A3C on all environments. **MinAtar.** Figure 4 summarize the results for Minatar [Bellemare et al., 2013, Young and Tian, 2019]. We see that VSOP beats PPO on 1 of the 4 environments, and that VSOP beats A3C on 2 of the 4 environments. **Classic Control.** We find that all methods perform equally well on the simple Classic Control benchmark and report our results in Appendix C.3.

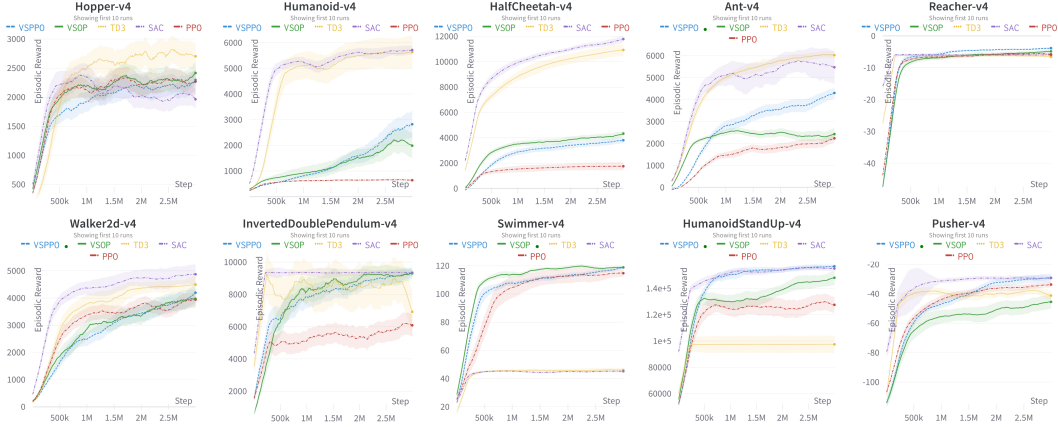


Figure 3: Mujoco continuous control benchmark comparison to SAC and TD3

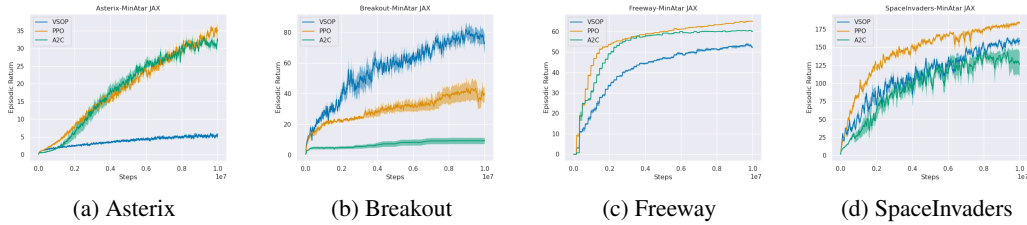


Figure 4: MinAtar Environments [Young and Tian, 2019]. Here we show results for VSOP (Blue), PPO (Orange), and A3C (Green) for the MinAtar environments. We plot the mean episodic return and standard error measurement over 5 random seeds. Each method is tuned over several hyperparameters using Bayesian Optimization [Snoek et al., 2012] with a budget of 100 search steps. We see that VSOP beats PPO on 1 of the 4 environments, and that VSOP beats A3C on 2 of the 4 environments.

6 Conclusion

We have presented a novel approach for improving the performance of on-policy DRL algorithms through the explicit incorporation of cautious interaction. Our method, realized through simple modifications to the A3C algorithm, optimizes a lower bound on the true value function plus a constant and integrates exploration via Thompson sampling. Significantly, we provide a theoretical justification for our approach by demonstrating that our algorithm indeed optimizes this lower bound. Our empirical evaluations across diverse benchmarks confirms our approach’s improved performance compared to existing on-policy algorithms. Although we acknowledge that achieving fully cautious algorithmic interaction with the world remains a distant goal, our research constitutes a significant stride towards this objective. We trust that our work will catalyze further advancements in the field, propelling the development of more cautious and effective DRL applications in resolving complex, real-world problems.

7 Broader Impact

Algorithmic decision making is becoming increasingly present in many areas of our life. While this has the potential for benefit, it also has also been shown that it can automate an perpetuate historical patterns that are often unjust and discriminatory [Birhane, 2021]. We believe that cautious interaction is a necessary feature for the type of deployed algorithmic decision making systems the RL community envisions, but believe that technological solutions alone will not suffice.

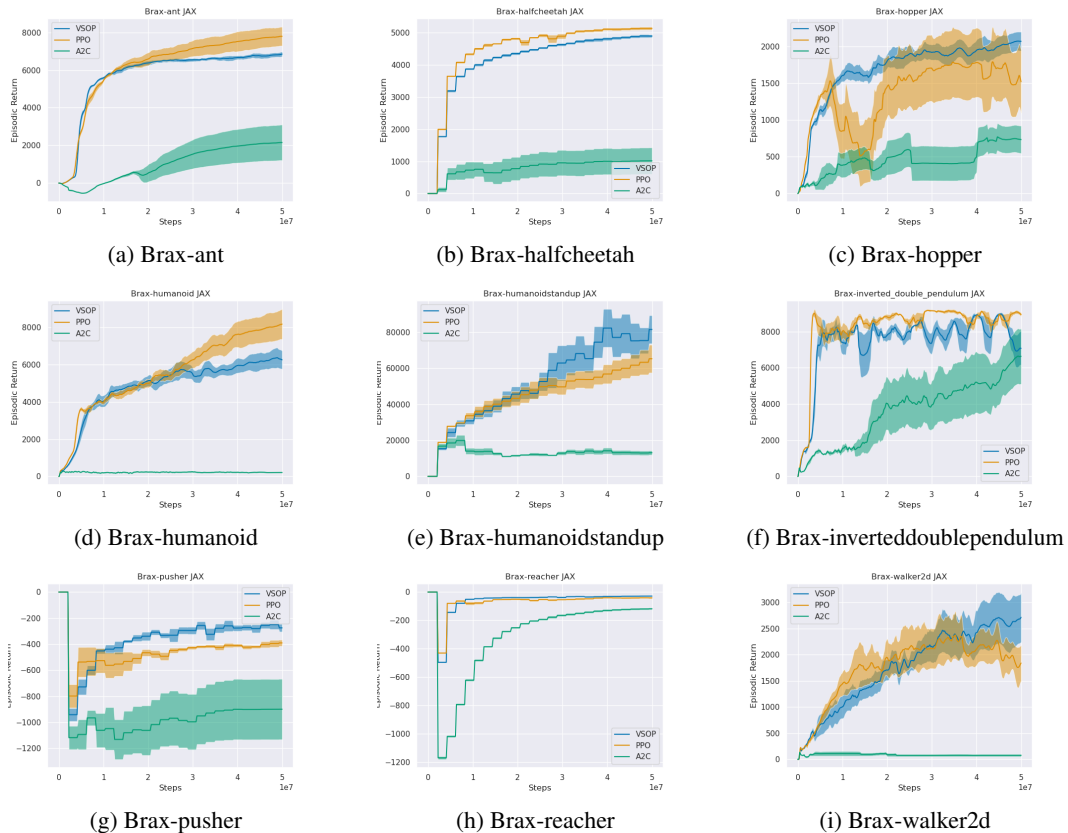


Figure 5: Brax-Mujoco Environments [Freeman et al., 2021, Todorov et al., 2012]. Here we show results for VSOP (Blue), PPO (Orange), and A3C (Green) for the Brax-Mujoco environments. We plot the mean episodic return and standard error measurement over 5 random seeds. Each method is tuned over several hyper-parameters using Bayesian Optimization [Snoek et al., 2012] with a budget of 100 search steps. We see that VSOP beats PPO on 5 of the 9 environments, and that VSOP beats A3C on all environments.

8 Acknowledgements

AJ would like to thank Luisa Zintgraf and Panagiotis Tigas for the crash course in reinforcement learning. This work began as a [twitter thread](#) and the authors would like to thank everyone who engaged. Specifically, we would like to thank Johan Ferret for highlighting connections to Self-Imitation Advantage Learning, Wilka Carvalho for highlighting connections to Self-Imitation Learning, Nathan Grinsztajn for highlighting connections to Risk Seeking Policy Gradients, Ohad Rubin for highlighting connections to Discovered Policy Optimization, and Marc Lanctot for the detailed discussion on Regret Matching Policy Gradients. Finally, the authors would like to thank Jannik Kossen for brainstorming the title.

References

- Navid Aghasadeghi and Timothy Bretl. Maximum entropy inverse reinforcement learning in continuous state spaces with path integrals. In *2011 IEEE/RSJ International Conference on Intelligent Robots and Systems*, pages 1561–1566. IEEE, 2011.
- Marcin Andrychowicz, Anton Raichuk, Piotr Stańczyk, Manu Orsini, Sertan Girgin, Raphaël Marinier, Leonard Hussenot, Matthieu Geist, Olivier Pietquin, Marcin Michalski, et al. What matters for on-policy deep actor-critic methods? a large-scale study. In *International conference on learning representations*, 2021.

- Kai Arulkumaran, Antoine Cully, and Julian Togelius. Alphastar: An evolutionary computation perspective. In *Proceedings of the genetic and evolutionary computation conference companion*, pages 314–315, 2019.
- Kamyar Azizzadenesheli, Emma Brunskill, and Animashree Anandkumar. Efficient exploration through bayesian deep q-networks. In *2018 Information Theory and Applications Workshop (ITA)*, pages 1–9. IEEE, 2018.
- Jimmy Lei Ba, Jamie Ryan Kiros, and Geoffrey E Hinton. Layer normalization. *arXiv preprint arXiv:1607.06450*, 2016.
- Philip J Ball, Laura Smith, Ilya Kostrikov, and Sergey Levine. Efficient online reinforcement learning with offline data. *arXiv preprint arXiv:2302.02948*, 2023.
- Marc G Bellemare, Yavar Naddaf, Joel Veness, and Michael Bowling. The arcade learning environment: An evaluation platform for general agents. *Journal of Artificial Intelligence Research*, 47: 253–279, 2013.
- Marc G Bellemare, Will Dabney, and Rémi Munos. A distributional perspective on reinforcement learning. In *International conference on machine learning*, pages 449–458. PMLR, 2017.
- Weights & Biases. Weights & biases. <https://wandb.ai/site>, 2018.
- Abeba Birhane. Algorithmic injustice: a relational ethics approach. *Patterns*, 2(2):100205, 2021.
- Nils Bjorck, Carla P Gomes, and Kilian Q Weinberger. Towards deeper deep reinforcement learning with spectral normalization. *Advances in Neural Information Processing Systems*, 34:8242–8255, 2021.
- James Bradbury, Roy Frostig, Peter Hawkins, Matthew James Johnson, Chris Leary, Dougal Maclaurin, George Necula, Adam Paszke, Jake VanderPlas, Skye Wanderman-Milne, and Qiao Zhang. JAX: composable transformations of Python+NumPy programs, 2018. URL <http://github.com/google/jax>.
- Greg Brockman, Vicki Cheung, Ludwig Pettersson, Jonas Schneider, John Schulman, Jie Tang, and Wojciech Zaremba. Openai gym. *arXiv preprint arXiv:1606.01540*, 2016.
- Kamil Ciosek, Quan Vuong, Robert Loftin, and Katja Hofmann. Better exploration with optimistic actor critic. *Advances in Neural Information Processing Systems*, 32, 2019.
- William R Clements, Bastien Van Delft, Benoît-Marie Robaglia, Reda Bahi Slaoui, and Sébastien Thot. Estimating risk and uncertainty in deep reinforcement learning. *arXiv preprint arXiv:1905.09638*, 2019.
- Logan Engstrom, Andrew Ilyas, Shibani Santurkar, Dimitris Tsipras, Firdaus Janoos, Larry Rudolph, and Aleksander Madry. Implementation matters in deep policy gradients: A case study on ppo and trpo. In *International Conference on Learning Representations*, 2020.
- Johan Ferret, Olivier Pietquin, and Matthieu Geist. Self-imitation advantage learning. *arXiv preprint arXiv:2012.11989*, 2020.
- Angelos Filos, Eszter Vértés, Zita Marinho, Gregory Farquhar, Diana Borsa, Abram Friesen, Feryal Behbahani, Tom Schaul, Andre Barreto, and Simon Osindero. Model-value inconsistency as a signal for epistemic uncertainty. In *International Conference on Machine Learning*, pages 6474–6498. PMLR, 2022.
- C. Daniel Freeman, Erik Frey, Anton Raichuk, Sertan Girgin, Igor Mordatch, and Olivier Bachem. Brax - a differentiable physics engine for large scale rigid body simulation, 2021. URL <http://github.com/google/brax>.
- Scott Fujimoto, Herke Hoof, and David Meger. Addressing function approximation error in actor-critic methods. In *International conference on machine learning*, pages 1587–1596. PMLR, 2018.

- Yarin Gal and Zoubin Ghahramani. Dropout as a bayesian approximation: Representing model uncertainty in deep learning. In *international conference on machine learning*, pages 1050–1059. PMLR, 2016.
- Florin Gogianu, Tudor Berariu, Mihaela C Rosca, Claudia Clopath, Lucian Busoniu, and Razvan Pascanu. Spectral normalisation for deep reinforcement learning: an optimisation perspective. In *International Conference on Machine Learning*, pages 3734–3744. PMLR, 2021.
- Ido Greenberg, Yinlam Chow, Mohammad Ghavamzadeh, and Shie Mannor. Efficient risk-averse reinforcement learning. *arXiv preprint arXiv:2205.05138*, 2022.
- Tuomas Haarnoja, Aurick Zhou, Pieter Abbeel, and Sergey Levine. Soft actor-critic: Off-policy maximum entropy deep reinforcement learning with a stochastic actor. In *International conference on machine learning*, pages 1861–1870. PMLR, 2018.
- Danijar Hafner, Timothy Lillicrap, Jimmy Ba, and Mohammad Norouzi. Dream to control: Learning behaviors by latent imagination. *arXiv preprint arXiv:1912.01603*, 2019.
- Mikael Henaff, Roberta Raileanu, Minqi Jiang, and Tim Rocktäschel. Exploration via elliptical episodic bonuses. In *Advances in Neural Information Processing Systems*.
- Geoffrey Hinton, Nitish Srivastava, and Kevin Swersky. Neural networks for machine learning. Lecture Slides, 2012. URL http://www.cs.toronto.edu/~tijmen/csc321/slides/lecture_slides_lec6.pdf.
- Shengyi Huang, Rousslan Fernand Julien Dossa, Chang Ye, Jeff Braga, Dipam Chakraborty, Kinal Mehta, and João G.M. Araújo. Cleanrl: High-quality single-file implementations of deep reinforcement learning algorithms. *Journal of Machine Learning Research*, 23(274):1–18, 2022. URL <http://jmlr.org/papers/v23/21-1342.html>.
- Julian Ibarz, Jie Tan, Chelsea Finn, Mrinal Kalakrishnan, Peter Pastor, and Sergey Levine. How to train your robot with deep reinforcement learning: lessons we have learned. *The International Journal of Robotics Research*, 40(4-5):698–721, 2021.
- Zachary Kenton, Angelos Filos, Owain Evans, and Yarin Gal. Generalizing from a few environments in safety-critical reinforcement learning. *arXiv preprint arXiv:1907.01475*, 2019.
- Diederik P Kingma and Jimmy Ba. Adam: A method for stochastic optimization. *arXiv preprint arXiv:1412.6980*, 2014.
- B Ravi Kiran, Ibrahim Sobh, Victor Talpaert, Patrick Mannion, Ahmad A Al Sallab, Senthil Yogamani, and Patrick Pérez. Deep reinforcement learning for autonomous driving: A survey. *IEEE Transactions on Intelligent Transportation Systems*, 23(6):4909–4926, 2021.
- Ilya Kostrikov, Denis Yarats, and Rob Fergus. Image augmentation is all you need: Regularizing deep reinforcement learning from pixels. *arXiv preprint arXiv:2004.13649*, 2020.
- Jakub Grudzien Kuba, Christian Schroeder de Witt, and Jakob Foerster. Mirror learning: A unifying framework of policy optimisation. *arXiv preprint arXiv:2201.02373*, 2022.
- Aviral Kumar, Aurick Zhou, George Tucker, and Sergey Levine. Conservative q-learning for offline reinforcement learning. *Advances in Neural Information Processing Systems*, 33:1179–1191, 2020.
- Robert Tjarko Lange. gymmax: A JAX-based reinforcement learning environment library, 2022. URL <http://github.com/RobertTLange/gymmax>.
- Timothy P Lillicrap, Jonathan J Hunt, Alexander Pritzel, Nicolas Heess, Tom Erez, Yuval Tassa, David Silver, and Daan Wierstra. Continuous control with deep reinforcement learning. *arXiv preprint arXiv:1509.02971*, 2015.
- Chris Lu, Jakub Kuba, Alistair Letcher, Luke Metz, Christian Schroeder de Witt, and Jakob Foerster. Discovered policy optimisation. *Advances in Neural Information Processing Systems*, 35:16455–16468, 2022.

- Takeru Miyato, Toshiki Kataoka, Masanori Koyama, and Yuichi Yoshida. Spectral normalization for generative adversarial networks. *arXiv preprint arXiv:1802.05957*, 2018.
- Volodymyr Mnih, Koray Kavukcuoglu, David Silver, Andrei A Rusu, Joel Veness, Marc G Bellemare, Alex Graves, Martin Riedmiller, Andreas K Fidjeland, Georg Ostrovski, et al. Human-level control through deep reinforcement learning. *nature*, 518(7540):529–533, 2015.
- Volodymyr Mnih, Adria Puigdomenech Badia, Mehdi Mirza, Alex Graves, Timothy Lillicrap, Tim Harley, David Silver, and Koray Kavukcuoglu. Asynchronous methods for deep reinforcement learning. In *International conference on machine learning*, pages 1928–1937. PMLR, 2016.
- Thomas M Moerland, Joost Broekens, and Catholijn M Jonker. Efficient exploration with double uncertain value networks. *arXiv preprint arXiv:1711.10789*, 2017.
- Vinod Nair and Geoffrey E Hinton. Rectified linear units improve restricted boltzmann machines. *Proceedings of the 27th international conference on machine learning (ICML-10)*, pages 807–814, 2010.
- Nikolay Nikolov, Johannes Kirschner, Felix Berkenkamp, and Andreas Krause. Information-directed exploration for deep reinforcement learning. *arXiv preprint arXiv:1812.07544*, 2018.
- Junhyuk Oh, Yijie Guo, Satinder Singh, and Honglak Lee. Self-imitation learning. In *International Conference on Machine Learning*, pages 3878–3887. PMLR, 2018.
- Ian Osband, Charles Blundell, Alexander Pritzel, and Benjamin Van Roy. Deep exploration via bootstrapped dqn. *Advances in neural information processing systems*, 29, 2016.
- Adam Paszke, Sam Gross, Soumith Chintala, Gregory Chanan, Edward Yang, Zachary DeVito, Zeming Lin, Alban Desmaison, Luca Antiga, and Adam Lerer. Pytorch: An imperative style, high-performance deep learning library. <https://pytorch.org>, 2019.
- Brenden K Petersen, Mikel Landajuela, T Nathan Mundhenk, Claudio P Santiago, Soo K Kim, and Joanne T Kim. Deep symbolic regression: Recovering mathematical expressions from data via risk-seeking policy gradients. *arXiv preprint arXiv:1912.04871*, 2019.
- LA Prashanth, Michael C Fu, et al. Risk-sensitive reinforcement learning via policy gradient search. *Foundations and Trends® in Machine Learning*, 15(5):537–693, 2022.
- Martin L Puterman. *Markov decision processes: discrete stochastic dynamic programming*. John Wiley & Sons, 2014.
- Antonin Raffin, Ashley Hill, Adam Gleave, Anssi Kanervisto, Maximilian Ernestus, and Noah Dormann. Stable-baselines3: Reliable reinforcement learning implementations. *Journal of Machine Learning Research*, 22(268):1–8, 2021. URL <http://jmlr.org/papers/v22/20-1364.html>.
- Aravind Rajeswaran, Sarvjeet Ghotra, Balaraman Ravindran, and Sergey Levine. Epopt: Learning robust neural network policies using model ensembles. *arXiv preprint arXiv:1610.01283*, 2016.
- Herbert Robbins and Sutton Monro. A stochastic approximation method. *The annals of mathematical statistics*, pages 400–407, 1951.
- John Schulman, Sergey Levine, Pieter Abbeel, Michael Jordan, and Philipp Moritz. Trust region policy optimization. In *International conference on machine learning*, pages 1889–1897. PMLR, 2015a.
- John Schulman, Philipp Moritz, Sergey Levine, Michael Jordan, and Pieter Abbeel. High-dimensional continuous control using generalized advantage estimation. *arXiv preprint arXiv:1506.02438*, 2015b.
- John Schulman, Filip Wolski, Prafulla Dhariwal, Alec Radford, and Oleg Klimov. Proximal policy optimization algorithms. *arXiv preprint arXiv:1707.06347*, 2017.
- David Silver, Julian Schrittwieser, Karen Simonyan, Ioannis Antonoglou, Aja Huang, Arthur Guez, Thomas Hubert, Lucas Baker, Matthew Lai, Adrian Bolton, et al. Mastering the game of go without human knowledge. *nature*, 550(7676):354–359, 2017.

- Jasper Snoek, Hugo Larochelle, and Ryan P Adams. Practical bayesian optimization of machine learning algorithms. *Advances in neural information processing systems*, 25, 2012.
- Sriram Srinivasan, Marc Lanctot, Vinicius Zambaldi, Julien Pérolat, Karl Tuyls, Rémi Munos, and Michael Bowling. Actor-critic policy optimization in partially observable multiagent environments. *Advances in neural information processing systems*, 31, 2018.
- Malcolm Strens. A bayesian framework for reinforcement learning. In *ICML*, volume 2000, pages 943–950, 2000.
- Richard S Sutton and Andrew G Barto. *Reinforcement learning: An introduction*. MIT press, 2018.
- Richard S Sutton, David McAllester, Satinder Singh, and Yishay Mansour. Policy gradient methods for reinforcement learning with function approximation. *Advances in neural information processing systems*, 12, 1999.
- Aviv Tamar, Yonatan Glassner, and Shie Mannor. Optimizing the cvar via sampling. In *Proceedings of the AAAI Conference on Artificial Intelligence*, volume 29, 2015.
- Yichuan Charlie Tang, Jian Zhang, and Ruslan Salakhutdinov. Worst cases policy gradients. In *Conference on Robot Learning*, pages 1078–1093. PMLR, 2020.
- William R Thompson. On the likelihood that one unknown probability exceeds another in view of the evidence of two samples. *Biometrika*, 25(3-4):285–294, 1933.
- Emanuel Todorov, Tom Erez, and Yuval Tassa. Mujoco: A physics engine for model-based control. <http://www.mujoco.org>, 2012.
- Tao Wang, Daniel Lizotte, Michael Bowling, and Dale Schuurmans. Bayesian sparse sampling for on-line reward optimization. In *Proceedings of the 22nd international conference on Machine learning*, pages 956–963, 2005.
- Ziyu Wang, Tom Schaul, Matteo Hessel, Hado Hasselt, Marc Lanctot, and Nando Freitas. Dueling network architectures for deep reinforcement learning. In *International conference on machine learning*, pages 1995–2003. PMLR, 2016.
- Travis Willse. What is the inverse operation of a gradient? Mathematics Stack Exchange, 2019. URL <https://math.stackexchange.com/q/3111825>. URL:<https://math.stackexchange.com/q/3111825> (version: 2019-02-13).
- Duo Xu and Faramarz Fekri. Improving actor-critic reinforcement learning via hamiltonian monte carlo method. *IEEE Transactions on Artificial Intelligence*, 2022.
- Kenny Young and Tian Tian. Minatar: An atari-inspired testbed for thorough and reproducible reinforcement learning experiments. *arXiv preprint arXiv:1903.03176*, 2019.
- Daniel M Ziegler, Nisan Stiennon, Jeffrey Wu, Tom B Brown, Alec Radford, Dario Amodei, Paul Christiano, and Geoffrey Irving. Fine-tuning language models from human preferences. *arXiv preprint arXiv:1909.08593*, 2019.

A Theoretical Results

A.1 Proof of Theorem 1

Theorem A.1. Let, $G_t := \sum_{k=t+1}^T \gamma^{k-1-t} R_k$, denote the discounted return. Let $q_\pi(\mathbf{s}, \mathbf{a}) = \mathbb{E}_\pi [G_t | \mathbf{S}_t = \mathbf{s}, \mathbf{A}_t = \mathbf{a}]$, denote the state-action value function, and $v_\pi(\mathbf{s}) = \mathbb{E}_\pi [G_t | \mathbf{S}_t = \mathbf{s}]$, denote the state value function, under policy $\pi(\mathbf{a} | \mathbf{s}, \boldsymbol{\theta})$. Let $(x)^+ := \max(0, x)$. Assume, without loss of generality, that rewards, R_t , are non-negative. Assume that the gradient of the policy, $\nabla \pi(\mathbf{a} | \mathbf{s}, \boldsymbol{\theta})$, is a conservative vector field. Then, performing gradient ascent with respect to,

$$\nabla_{\boldsymbol{\theta}} J(\boldsymbol{\theta}) = \mathbb{E}_\pi \left[\left(q_\pi(\mathbf{S}_t, \mathbf{A}_t) - v_\pi(\mathbf{S}_t) \right)^+ \nabla_{\boldsymbol{\theta}} \log \pi(\mathbf{A}_t | \mathbf{S}_t, \boldsymbol{\theta}) \right], \quad (4)$$

maximizes a lower-bound, $v_\pi^*(\mathbf{s})$, on the state value function, $v_\pi(\mathbf{s})$, plus a constant:

$$v_\pi^*(\mathbf{s}) \leq v_\pi(\mathbf{s}) + C(\mathbf{s}), \quad (5)$$

where, $C(\mathbf{s}) = \iint \left(\gamma v_\pi(\mathbf{s}') - v_\pi(\mathbf{s}) \right)^+ d\mathbb{P}(\mathbf{s}' | \mathbf{S}_t = \mathbf{s}, \mathbf{A}_t = \mathbf{a}) d\Pi(\mathbf{a} | \mathbf{S}_t = \mathbf{s})$, is the expected, clipped difference in the state value function, $\gamma v_\pi(\mathbf{s}') - v_\pi(\mathbf{s})$, over all actions, \mathbf{a} , and next states, \mathbf{s}' , under the policy given state, \mathbf{s} . Here, we use $\int \dots d\Pi(\mathbf{a} | \mathbf{s})$ to denote $\sum_{\mathbf{a}} \dots \pi(\mathbf{a} | \mathbf{s})$ for discrete action spaces and $\int \dots \pi(\mathbf{a} | \mathbf{s}) d\mathbf{a}$ for continuous action spaces. Similarly, we use $\int \dots d\mathbb{P}(\mathbf{s}' | \mathbf{s}, \mathbf{a})$ to denote $\sum_{\mathbf{s}'} \dots p(\mathbf{s}' | \mathbf{s}, \mathbf{a})$ for discrete state spaces and $\int \dots p(\mathbf{s}' | \mathbf{s}, \mathbf{a}) d\mathbf{s}'$ for continuous state spaces.

Proof. Corollary A.1 shows that the policy-gradient theorem [Sutton et al., 1999] can be expressed in terms of the clipped advantage function,

$$h_\pi^+(\mathbf{s}, \mathbf{a}) = \left(q_\pi(\mathbf{s}, \mathbf{a}) - v_\pi(\mathbf{s}) \right)^+ := \max(0, q_\pi(\mathbf{s}, \mathbf{a}) - v_\pi(\mathbf{s})),$$

as,

$$\begin{aligned} \nabla v_\pi(\mathbf{s}) &= \int_{\mathcal{S}} \sum_{k=0}^{\infty} \left[\gamma^k \int_{\mathcal{A}} h_\pi^+(\mathbf{x}, \mathbf{a}) \nabla d\Pi(\mathbf{a} | \mathbf{x}) \right] d\mathbb{P}(\mathbf{s} \rightarrow \mathbf{x}; k, \pi) \\ &\quad + \int_{\mathcal{S}} \sum_{k=0}^{\infty} \left[\gamma^k \int_{\mathcal{A}} \mathbb{1}(q_\pi(\mathbf{x}, \mathbf{a}) > v_\pi(\mathbf{x})) v_\pi(\mathbf{x}) \nabla d\Pi(\mathbf{a} | \mathbf{x}) \right] d\mathbb{P}(\mathbf{s} \rightarrow \mathbf{x}; k, \pi) \\ &\quad + \int_{\mathcal{S}} \sum_{k=0}^{\infty} \left[\gamma^k \int_{\mathcal{A}} \mathbb{1}(q_\pi(\mathbf{x}, \mathbf{a}) \leq v_\pi(\mathbf{x})) q_\pi(\mathbf{x}, \mathbf{a}) \nabla d\Pi(\mathbf{a} | \mathbf{x}) \right] d\mathbb{P}(\mathbf{s} \rightarrow \mathbf{x}; k, \pi), \end{aligned} \quad (6)$$

where, $\mathbb{P}(\mathbf{s} \rightarrow \mathbf{x}; k, \pi)$, is the probability of transitioning from state \mathbf{s} to state \mathbf{x} in k steps under policy π .

The first right hand side term above defines the gradient of the lower-bound, $v_\pi^*(\mathbf{s})$, with respect to $\boldsymbol{\theta}$:

$$\nabla v_\pi^*(\mathbf{s}) := \int_{\mathcal{S}} \sum_{k=0}^{\infty} \left[\gamma^k \int_{\mathcal{A}} h_\pi^+(\mathbf{x}, \mathbf{a}) \nabla d\Pi(\mathbf{a} | \mathbf{x}) \right] d\mathbb{P}(\mathbf{s} \rightarrow \mathbf{x}; k, \pi). \quad (7)$$

Letting, $v_\pi^*(\mathbf{s}_0) = \int_{\mathcal{S}} \sum_{k=0}^{\infty} \gamma^k \int_{\mathcal{A}} h_\pi^+(\mathbf{s}, \mathbf{a}) \nabla d\Pi(\mathbf{a} | \mathbf{s}) d\mathbb{P}(\mathbf{s}_0 \rightarrow \mathbf{s}; k, \pi)$, a straightforward continuation of the policy gradient theorem [Sutton et al., 1999] will show that

$$\nabla J(\boldsymbol{\theta}) := \nabla v_\pi^*(\mathbf{s}_0) \propto \iint h_\pi^+(\mathbf{s}, \mathbf{a}) \nabla_{\boldsymbol{\theta}} d\Pi(\mathbf{a} | \mathbf{s}, \boldsymbol{\theta}) d\mathbb{P}(\mathbf{s}).$$

We then arrive at Equation (4) by moving from the all states/actions to single state/action formulation:

$$\begin{aligned}
\nabla J(\boldsymbol{\theta}) &:= \nabla v_\pi^*(\mathbf{s}_0), && \text{by definition} \\
&\propto \iint \left(q_\pi(\mathbf{s}, \mathbf{a}) - v_\pi(\mathbf{s}) \right)^+ \nabla_{\boldsymbol{\theta}} d\Pi(\mathbf{a} \mid \mathbf{s}, \boldsymbol{\theta}) d\mathbb{P}(\mathbf{s}), && \text{Sutton et al. [1999]} \\
&= \mathbb{E}_\pi \left[\int \left(q_\pi(\mathbf{S}_t, \mathbf{a}) - v_\pi(\mathbf{S}_t) \right)^+ \nabla_{\boldsymbol{\theta}} d\Pi(\mathbf{a} \mid \mathbf{S}_t, \boldsymbol{\theta}) \right], \\
&= \mathbb{E}_\pi \left[\int \left(q_\pi(\mathbf{S}_t, \mathbf{a}) - v_\pi(\mathbf{S}_t) \right)^+ \frac{\nabla_{\boldsymbol{\theta}} d\Pi(\mathbf{a} \mid \mathbf{S}_t, \boldsymbol{\theta})}{d\Pi(\mathbf{a} \mid \mathbf{S}_t, \boldsymbol{\theta})} d\Pi(\mathbf{a} \mid \mathbf{S}_t, \boldsymbol{\theta}) \right], \\
&= \mathbb{E}_\pi \left[\int \left(q_\pi(\mathbf{S}_t, \mathbf{A}_t) - v_\pi(\mathbf{S}_t) \right)^+ \nabla_{\boldsymbol{\theta}} \log \pi(\mathbf{A}_t \mid \mathbf{S}_t, \boldsymbol{\theta}) \right].
\end{aligned}$$

Now we need to show that,

$$v_\pi^*(\mathbf{s}) \leq v_\pi(\mathbf{s}) + \iint \left(\gamma v_\pi(\mathbf{s}') - v_\pi(\mathbf{s}) \right)^+ d\mathbb{P}(\mathbf{s}' \mid \mathbf{S}_t = \mathbf{s}, \mathbf{A}_t) d\Pi(\mathbf{a} \mid \mathbf{S}_t = \mathbf{s}).$$

To do so, we will first prove that it holds for episodes, \mathbb{T} , of length 1, then that it holds for episodes of length 2. These two proofs will then prove Equation (5) for episodes of arbitrary length by mathematical induction and conclude the proof.

For episodes of length 1, $|\mathbb{T}| = 1$, we have

$$\begin{aligned}
\nabla v_\pi(\mathbf{s}) &= \int q_\pi(\mathbf{s}, \mathbf{a}) \nabla d\Pi(\mathbf{a} \mid \mathbf{s}) + \int \nabla q_\pi(\mathbf{s}, \mathbf{a}) d\Pi(\mathbf{a} \mid \mathbf{s}), \\
&= \int q_\pi(\mathbf{s}, \mathbf{a}) \nabla d\Pi(\mathbf{a} \mid \mathbf{s}) + \int \left(\nabla \int r d\mathbb{P}(r \mid \mathbf{s}, \mathbf{a}) \right) d\Pi(\mathbf{a} \mid \mathbf{s}), \\
&= \int q_\pi(\mathbf{s}, \mathbf{a}) \nabla d\Pi(\mathbf{a} \mid \mathbf{s}), \\
&= \int h_\pi^+(\mathbf{s}, \mathbf{a}) \nabla d\Pi(\mathbf{a} \mid \mathbf{s}) + \int \left(\mathbb{1}(q_\pi > v_\pi) v_\pi(\mathbf{s}) + \mathbb{1}(q_\pi \leq v_\pi) q_\pi(\mathbf{s}, \mathbf{a}) \right) \nabla d\Pi(\mathbf{a} \mid \mathbf{s}).
\end{aligned} \tag{9}$$

Therefore, for $|\mathbb{T}| = 1$,

$$\nabla v_\pi^*(\mathbf{s}) = \int h_\pi^+(\mathbf{s}, \mathbf{a}) \nabla d\Pi(\mathbf{a} \mid \mathbf{s})$$

In order to recover $v_\pi^*(\mathbf{s})$, we need to use the work of Willse [2019] to define an inverse function for the gradient. Assume that the policy, $\pi(\mathbf{a} \mid \mathbf{s}, \boldsymbol{\theta})$, is a smooth, infinitely differentiable function with respect to $\boldsymbol{\theta}$. Further, let the gradient of the policy,

$$\nabla \pi(\mathbf{a} \mid \mathbf{s}, \boldsymbol{\theta}) = \begin{pmatrix} \frac{\partial}{\partial \theta_1} \pi(\mathbf{a} \mid \mathbf{s}, \theta_1), \\ \vdots \\ \frac{\partial}{\partial \theta_k} \pi(\mathbf{a} \mid \mathbf{s}, \theta_k) \end{pmatrix}, \tag{10}$$

be a conservative vector field. We call $\tilde{\beta}(\nabla \pi(\mathbf{a} \mid \mathbf{s}, \boldsymbol{\theta}))$ the inverse of the gradient operation, $\nabla \pi(\mathbf{a} \mid \mathbf{s}, \boldsymbol{\theta})$. Assuming that $\pi(\mathbf{a} \mid \mathbf{s}, \boldsymbol{\theta})$ is a representative of $\tilde{\beta}$, we have that,

$$\begin{aligned}
\pi(\mathbf{a} \mid \mathbf{s}, \boldsymbol{\theta}) &= \tilde{\beta}(\nabla \pi(\mathbf{a} \mid \mathbf{s}, \boldsymbol{\theta})), \\
&= \int_\gamma \nabla \pi(\mathbf{a} \mid \mathbf{s}, \boldsymbol{\theta}) dx, \\
&= \int_\gamma \frac{\partial}{\partial \theta_1} \pi(\mathbf{a} \mid \mathbf{s}, \theta_1) d\theta_1 + \cdots + \frac{\partial}{\partial \theta_k} \pi(\mathbf{a} \mid \mathbf{s}, \theta_k) d\theta_k,
\end{aligned} \tag{11}$$

where γ is a path from the fixed reference point, $\boldsymbol{\theta}_0$, to $\boldsymbol{\theta}$. The conservativeness of $\nabla \pi(\mathbf{a} \mid \mathbf{s}, \boldsymbol{\theta})$ guarantees that the integrals are path independent.

Now we have,

$$\begin{aligned}
v_\pi^*(\mathbf{s}) &= \tilde{\beta} \left(\int h_\pi^+(\mathbf{s}, \mathbf{a}) \nabla d\Pi(\mathbf{a} | \mathbf{s}) \right), \\
&= \int h_\pi^+(\mathbf{s}, \mathbf{a}) \tilde{\beta}(\nabla d\Pi(\mathbf{a} | \mathbf{s})), && \text{linearity} \\
&= \int h_\pi^+(\mathbf{s}, \mathbf{a}) d\Pi(\mathbf{a} | \mathbf{s}), && \text{Equation (11)} \\
&\leq \iint (\mathbf{r} + (\gamma v_\pi(\mathbf{s}') - v_\pi(\mathbf{s}))^+) d\mathbb{P}(\mathbf{s}', \mathbf{r} | \mathbf{s}, \mathbf{a}) d\Pi(\mathbf{a} | \mathbf{s}), && \text{Corollary A.2} \\
&= v_\pi(\mathbf{s}) + \iint (\gamma v_\pi(\mathbf{s}') - v_\pi(\mathbf{s}))^+ d\mathbb{P}(\mathbf{s}' | \mathbf{s}, \mathbf{a}) d\Pi(\mathbf{a} | \mathbf{s}), && |\mathbb{T}| = 1
\end{aligned}$$

which concludes the proof for episodes of length 1.

For episodes of length 2, $|T| = 2$, we have

$$\begin{aligned}
\nabla v_\pi(\mathbf{s}) &= \int q_\pi(\mathbf{s}, \mathbf{a}) \nabla d\Pi(\mathbf{a} | \mathbf{s}) + \int \nabla q_\pi(\mathbf{s}, \mathbf{a}) d\Pi(\mathbf{a} | \mathbf{s}), \\
&= \int q_\pi(\mathbf{s}, \mathbf{a}) \nabla d\Pi(\mathbf{a} | \mathbf{s}) + \iiint q_\pi(\mathbf{s}', \mathbf{a}') \nabla d\Pi(\mathbf{a}' | \mathbf{s}') d\mathbb{P}(\mathbf{s}' | \mathbf{a}, \mathbf{s}) d\Pi(\mathbf{a} | \mathbf{s}) \\
&\quad + \iiint \left(\nabla \int \mathbf{r}' d\mathbb{P}(\mathbf{r}' | \mathbf{s}', \mathbf{a}') \right) d\Pi(\mathbf{a}' | \mathbf{s}'), \\
&= \int q_\pi(\mathbf{s}, \mathbf{a}) \nabla d\Pi(\mathbf{a} | \mathbf{s}) + \iiint q_\pi(\mathbf{s}', \mathbf{a}') \nabla d\Pi(\mathbf{a}' | \mathbf{s}') d\mathbb{P}(\mathbf{s}' | \mathbf{a}, \mathbf{s}) d\Pi(\mathbf{a} | \mathbf{s}), \\
&= \int h_\pi^+(\mathbf{s}, \mathbf{a}) \nabla d\Pi(\mathbf{a} | \mathbf{s}) + \iiint h_\pi^+(\mathbf{s}', \mathbf{a}') \nabla d\Pi(\mathbf{a}' | \mathbf{s}') d\mathbb{P}(\mathbf{s}' | \mathbf{a}, \mathbf{s}) d\Pi(\mathbf{a} | \mathbf{s}) \\
&\quad + \int \left(\mathbf{1}(q_\pi > v_\pi) v_\pi(\mathbf{s}) + \mathbf{1}(q_\pi \leq v_\pi) q_\pi(\mathbf{s}, \mathbf{a}) \right) \nabla d\Pi(\mathbf{a} | \mathbf{s}) \\
&\quad + \iiint \left(\mathbf{1}(q_\pi > v_\pi) v_\pi(\mathbf{s}') + \mathbf{1}(q_\pi \leq v_\pi) q_\pi(\mathbf{s}', \mathbf{a}') \right) \nabla d\Pi(\mathbf{a}' | \mathbf{s}') d\mathbb{P}(\mathbf{s}' | \mathbf{a}, \mathbf{s}) d\Pi(\mathbf{a} | \mathbf{s}).
\end{aligned}$$

Therefore, for $|T| = 2$,

$$\nabla v_\pi^*(\mathbf{s}) = \int h_\pi^+(\mathbf{s}, \mathbf{a}) \nabla d\Pi(\mathbf{a} | \mathbf{s}) + \iiint h_\pi^+(\mathbf{s}', \mathbf{a}') \nabla d\Pi(\mathbf{a}' | \mathbf{s}') d\mathbb{P}(\mathbf{s}' | \mathbf{a}, \mathbf{s}) d\Pi(\mathbf{a} | \mathbf{s}).$$

Finally, we apply the $\tilde{\beta}$ operator:

$$\begin{aligned}
v_\pi^*(\mathbf{s}) &= \tilde{\beta} \left(\int h_\pi^+(\mathbf{s}, \mathbf{a}) \nabla d\Pi(\mathbf{a} | \mathbf{s}) + \iiint h_\pi^+(\mathbf{s}', \mathbf{a}') \nabla d\Pi(\mathbf{a}' | \mathbf{s}') d\mathbb{P}(\mathbf{s}' | \mathbf{a}, \mathbf{s}) d\Pi(\mathbf{a} | \mathbf{s}) \right), \\
&= \int h_\pi^+(\mathbf{s}, \mathbf{a}) \tilde{\beta}(\nabla d\Pi(\mathbf{a} | \mathbf{s})) + \iiint h_\pi^+(\mathbf{s}', \mathbf{a}') \tilde{\beta}(\nabla d\Pi(\mathbf{a}' | \mathbf{s}')) d\mathbb{P}(\mathbf{s}' | \mathbf{a}, \mathbf{s}) d\Pi(\mathbf{a} | \mathbf{s}), && \text{linearity} \\
&= \int h_\pi^+(\mathbf{s}, \mathbf{a}) d\Pi(\mathbf{a} | \mathbf{s}) + \iiint h_\pi^+(\mathbf{s}', \mathbf{a}') d\Pi(\mathbf{a}' | \mathbf{s}') d\mathbb{P}(\mathbf{s}' | \mathbf{a}, \mathbf{s}) d\Pi(\mathbf{a} | \mathbf{s}), && \text{Equation (11)} \\
&\leq \iint \mathbf{r} d\mathbb{P}(\mathbf{r} | \mathbf{s}, \mathbf{a}) d\Pi(\mathbf{a} | \mathbf{s}) + \iint (\gamma v_\pi(\mathbf{s}') - v_\pi(\mathbf{s}))^+ d\mathbb{P}(\mathbf{s}' | \mathbf{s}, \mathbf{a}) d\Pi(\mathbf{a} | \mathbf{s}) \\
&\quad + \iiint h_\pi^+(\mathbf{s}', \mathbf{a}') d\Pi(\mathbf{a}' | \mathbf{s}') d\mathbb{P}(\mathbf{s}' | \mathbf{a}, \mathbf{s}) d\Pi(\mathbf{a} | \mathbf{s}), && \text{Corollary A.2} \\
&\leq \iint \mathbf{r} d\mathbb{P}(\mathbf{r} | \mathbf{s}, \mathbf{a}) d\Pi(\mathbf{a} | \mathbf{s}) + \iint (\gamma v_\pi(\mathbf{s}') - v_\pi(\mathbf{s}))^+ d\mathbb{P}(\mathbf{s}' | \mathbf{s}, \mathbf{a}) d\Pi(\mathbf{a} | \mathbf{s}) \\
&\quad + \iint \gamma v_\pi(\mathbf{s}') d\mathbb{P}(\mathbf{s}' | \mathbf{a}, \mathbf{s}) d\Pi(\mathbf{a} | \mathbf{s}), && \text{Corollary A.3} \\
&= v_\pi(\mathbf{s}) + \iint (\gamma v_\pi(\mathbf{s}') - v_\pi(\mathbf{s}))^+ d\mathbb{P}(\mathbf{s}' | \mathbf{s}, \mathbf{a}) d\Pi(\mathbf{a} | \mathbf{s}). && \text{rearranging terms}
\end{aligned}$$

□

Corollary A.1. $\nabla v_\pi(\mathbf{s})$ can be written in terms of $h_\pi^+(\mathbf{s}, \mathbf{a})$.

Proof.

$$\nabla v_\pi(\mathbf{s}) = \nabla \left[\int q_\pi(\mathbf{s}, \mathbf{a}) d\Pi(\mathbf{a} | \mathbf{s}) \right], \quad (15a)$$

$$= \int q_\pi(\mathbf{s}, \mathbf{a}) \nabla d\Pi(\mathbf{a} | \mathbf{s}) + \int \nabla q_\pi(\mathbf{s}, \mathbf{a}) d\Pi(\mathbf{a} | \mathbf{s}), \quad (15b)$$

$$= \int \left(h_\pi^+(\mathbf{s}, \mathbf{a}) + \mathbf{1}(q_\pi > v_\pi) v_\pi(\mathbf{s}) + \mathbf{1}(q_\pi \leq v_\pi) q_\pi(\mathbf{s}, \mathbf{a}) \right) \nabla d\Pi(\mathbf{a} | \mathbf{s}) \\ + \int \nabla q_\pi(\mathbf{s}, \mathbf{a}) d\Pi(\mathbf{a} | \mathbf{s}), \quad (15c)$$

$$= \int \left(h_\pi^+(\mathbf{s}, \mathbf{a}) + \mathbf{1}(q_\pi > v_\pi) v_\pi(\mathbf{s}) + \mathbf{1}(q_\pi \leq v_\pi) q_\pi(\mathbf{s}, \mathbf{a}) \right) \nabla d\Pi(\mathbf{a} | \mathbf{s}) \\ + \int \nabla \left[\int (r + \gamma v_\pi(\mathbf{s}')) d\mathbb{P}(\mathbf{s}', r | \mathbf{s}, \mathbf{a}) \right] d\Pi(\mathbf{a} | \mathbf{s}), \quad (15d)$$

$$= \int \left(h_\pi^+(\mathbf{s}, \mathbf{a}) + \mathbf{1}(q_\pi > v_\pi) v_\pi(\mathbf{s}) + \mathbf{1}(q_\pi \leq v_\pi) q_\pi(\mathbf{s}, \mathbf{a}) \right) \nabla d\Pi(\mathbf{a} | \mathbf{s}) \\ + \gamma \iint \nabla v_\pi(\mathbf{s}') d\mathbb{P}(\mathbf{s}' | \mathbf{s}, \mathbf{a}) d\Pi(\mathbf{a} | \mathbf{s}), \quad (15e)$$

$$= \int \left(h_\pi^+(\mathbf{s}, \mathbf{a}) + \mathbf{1}(q_\pi > v_\pi) v_\pi(\mathbf{s}) + \mathbf{1}(q_\pi \leq v_\pi) q_\pi(\mathbf{s}, \mathbf{a}) \right) \nabla d\Pi(\mathbf{a} | \mathbf{s}) \\ + \gamma \iint \left[\int q_\pi(\mathbf{s}', \mathbf{a}') \nabla d\Pi(\mathbf{a}' | \mathbf{s}') \right. \\ \left. + \gamma \int \nabla v_\pi(\mathbf{s}'') d\mathbb{P}(\mathbf{s}'' | \mathbf{s}', \mathbf{a}') d\Pi(\mathbf{a}' | \mathbf{s}') \right] d\mathbb{P}(\mathbf{s}' | \mathbf{s}, \mathbf{a}) d\Pi(\mathbf{a} | \mathbf{s}), \quad (15f)$$

$$= \int \left(h_\pi^+(\mathbf{s}, \mathbf{a}) + \mathbf{1}(q_\pi > v_\pi) v_\pi(\mathbf{s}) + \mathbf{1}(q_\pi \leq v_\pi) q_\pi(\mathbf{s}, \mathbf{a}) \right) \nabla d\Pi(\mathbf{a} | \mathbf{s}) \\ + \gamma \iint \left[\int \left(h_\pi^+(\mathbf{s}', \mathbf{a}') + \mathbf{1}(q_\pi > v_\pi) v_\pi(\mathbf{s}') + \mathbf{1}(q_\pi \leq v_\pi) q_\pi(\mathbf{s}', \mathbf{a}') \right) \nabla d\Pi(\mathbf{a}' | \mathbf{s}') \right. \\ \left. + \gamma \int \nabla v_\pi(\mathbf{s}'') d\mathbb{P}(\mathbf{s}'' | \mathbf{s}', \mathbf{a}') d\Pi(\mathbf{a}' | \mathbf{s}') \right] d\mathbb{P}(\mathbf{s}' | \mathbf{s}, \mathbf{a}) d\Pi(\mathbf{a} | \mathbf{s}), \quad (15g)$$

$$= \int_{\mathcal{S}} \sum_{k=0}^{\infty} \left[\gamma^k \int_{\mathcal{A}} h_\pi^+(\mathbf{x}, \mathbf{a}) \nabla d\Pi(\mathbf{a} | \mathbf{x}) \right] d\mathbb{P}(\mathbf{s} \rightarrow \mathbf{x}; k, \pi) \\ + \int_{\mathcal{S}} \sum_{k=0}^{\infty} \left[\gamma^k \int_{\mathcal{A}} \mathbf{1}(q_\pi(\mathbf{x}, \mathbf{a}) > v_\pi(\mathbf{x})) v_\pi(\mathbf{x}) \nabla d\Pi(\mathbf{a} | \mathbf{x}) \right] d\mathbb{P}(\mathbf{s} \rightarrow \mathbf{x}; k, \pi) \\ + \int_{\mathcal{S}} \sum_{k=0}^{\infty} \left[\gamma^k \int_{\mathcal{A}} \mathbf{1}(q_\pi(\mathbf{x}, \mathbf{a}) \leq v_\pi(\mathbf{x})) q_\pi(\mathbf{x}, \mathbf{a}) \nabla d\Pi(\mathbf{a} | \mathbf{x}) \right] d\mathbb{P}(\mathbf{s} \rightarrow \mathbf{x}; k, \pi) \quad (15h)$$

□

Corollary A.2.

$$\underline{v}_\pi^{v_\pi}(\mathbf{s}) \leq \iint r d\mathbb{P}(r | \mathbf{s}, \mathbf{a}) d\Pi(\mathbf{a} | \mathbf{s}) + \iint \left(\gamma v_\pi(\mathbf{s}') - v_\pi(\mathbf{s}) \right)^+ d\mathbb{P}(\mathbf{s}' | \mathbf{s}, \mathbf{a}) d\Pi(\mathbf{a} | \mathbf{s})$$

Proof.

$$\begin{aligned}
\underline{v}_\pi^{v_\pi}(\mathbf{s}) &:= \int h_\pi^+(\mathbf{s}, \mathbf{a}) d\Pi(\mathbf{a} | \mathbf{s}) \\
&= \frac{1}{2} \int \left(q_\pi(\mathbf{s}, \mathbf{a}) - v_\pi + |q_\pi(\mathbf{s}, \mathbf{a}) - v_\pi| \right) d\Pi(\mathbf{a} | \mathbf{s}) && (2 \max(0, a) = a + |a|) \\
&= \frac{1}{2} \int \left(\int (\mathbf{r} + \gamma v_\pi(\mathbf{s}') - v_\pi(\mathbf{s})) d\mathbb{P}(\mathbf{s}', \mathbf{r} | \mathbf{s}, \mathbf{a}) \right. \\
&\quad \left. + \left| \int (\mathbf{r} + \gamma v_\pi(\mathbf{s}') - v_\pi(\mathbf{s})) d\mathbb{P}(\mathbf{s}', \mathbf{r} | \mathbf{s}, \mathbf{a}) \right| \right) d\Pi(\mathbf{a} | \mathbf{s}) \\
&\leq \frac{1}{2} \iint \left(\mathbf{r} + \gamma v_\pi(\mathbf{s}') - v_\pi(\mathbf{s}) + |\mathbf{r} + \gamma v_\pi(\mathbf{s}') - v_\pi(\mathbf{s})| \right) && (\text{Jensen's inequality}) \\
&\quad d\mathbb{P}(\mathbf{s}', \mathbf{r} | \mathbf{s}, \mathbf{a}) d\Pi(\mathbf{a} | \mathbf{s}) \\
&\leq \frac{1}{2} \iint \left(2\mathbf{r} + \gamma v_\pi(\mathbf{s}') - v_\pi(\mathbf{s}) + |\gamma v_\pi(\mathbf{s}') - v_\pi(\mathbf{s})| \right) && (\text{triangle inequality}) \\
&\quad d\mathbb{P}(\mathbf{s}', \mathbf{r} | \mathbf{s}, \mathbf{a}) d\Pi(\mathbf{a} | \mathbf{s}) \\
&= \iint \left(\mathbf{r} + (\gamma v_\pi(\mathbf{s}') - v_\pi(\mathbf{s}))^+ \right) d\mathbb{P}(\mathbf{s}', \mathbf{r} | \mathbf{s}, \mathbf{a}) d\Pi(\mathbf{a} | \mathbf{s}) && (2 \max(0, a) = a + |a|)
\end{aligned}$$

□

Corollary A.3. *When, without loss of generality, rewards, R_t , are assumed to be non-negative:*

$$\underline{v}_\pi^{v_\pi}(\mathbf{s}) := \int h_\pi^+(\mathbf{s}, \mathbf{a}) d\Pi(\mathbf{a} | \mathbf{s}) \leq v_\pi(\mathbf{s})$$

Proof.

$$\begin{aligned}
\int h_\pi^+(\mathbf{s}, \mathbf{a}) d\Pi(\mathbf{a} | \mathbf{s}) &= \frac{1}{2} \int \left(q_\pi(\mathbf{s}, \mathbf{a}) - v_\pi + |q_\pi(\mathbf{s}, \mathbf{a}) - v_\pi| \right) d\Pi(\mathbf{a} | \mathbf{s}) && (2 \max(0, a) = a + |a|) \\
&\leq \int q_\pi(\mathbf{s}, \mathbf{a}) d\Pi(\mathbf{a} | \mathbf{s}) && (\text{triangle inequality}) \\
&= v_\pi(\mathbf{s})
\end{aligned}$$

□

A.2 Relation to Regret Matching Policy Gradient (RMPG)

Here we provide a derivation starting from RMPG and arriving at our method.

$$\begin{aligned}
\nabla J(\boldsymbol{\theta}) &= \mathbb{E}_\pi \left[\int_{\mathcal{A}} \left(q_\pi(\mathbf{S}_t, \mathbf{a}) - \int_{\mathcal{A}} \pi(\mathbf{a}' | \mathbf{S}_t, \boldsymbol{\theta}) q_\pi(\mathbf{S}_t, \mathbf{a}') d\mathbf{a}' \right)^+ \nabla_{\boldsymbol{\theta}} \pi(\mathbf{a} | \mathbf{S}_t, \boldsymbol{\theta}) d\mathbf{a} \right] \\
&= \mathbb{E}_\pi \left[\int_{\mathcal{A}} (q_\pi(\mathbf{S}_t, \mathbf{a}) - v_\pi(\mathbf{S}_t))^+ \nabla_{\boldsymbol{\theta}} \pi(\mathbf{a} | \mathbf{S}_t, \boldsymbol{\theta}) d\mathbf{a} \right] \\
&= \mathbb{E}_\pi \left[\int_{\mathcal{A}} h_\pi^+(\mathbf{S}_t, \mathbf{a}) \nabla_{\boldsymbol{\theta}} \pi(\mathbf{a} | \mathbf{S}_t, \boldsymbol{\theta}) d\mathbf{a} \right] \\
&= \mathbb{E}_\pi \left[\int_{\mathcal{A}} \pi(\mathbf{a} | \mathbf{S}_t, \boldsymbol{\theta}) h_\pi^+(\mathbf{S}_t, \mathbf{a}) \frac{\nabla_{\boldsymbol{\theta}} \pi(\mathbf{a} | \mathbf{S}_t, \boldsymbol{\theta})}{\pi(\mathbf{a} | \mathbf{S}_t, \boldsymbol{\theta})} d\mathbf{a} \right] \\
&= \mathbb{E}_\pi \left[h_\pi^+(\mathbf{S}_t, \mathbf{A}_t) \frac{\nabla_{\boldsymbol{\theta}} \pi(\mathbf{A}_t | \mathbf{S}_t, \boldsymbol{\theta})}{\pi(\mathbf{A}_t | \mathbf{S}_t, \boldsymbol{\theta})} \right] \\
&= \mathbb{E}_\pi \left[h_\pi^+(\mathbf{S}_t, \mathbf{A}_t) \nabla_{\boldsymbol{\theta}} \log \pi(\mathbf{A}_t | \mathbf{S}_t, \boldsymbol{\theta}) \right]
\end{aligned}$$

B Implementation Details

We have attached the code that replicates the reported results in the folder “vsop-main” and will release a public github repo after the review process.

B.1 Gymnasium

We build off of Huang et al. [2022]’s CleanRL package which provides reproducible, user-friendly implementations of state-of-the-art reinforcement learning algorithms using PyTorch [Paszke et al., 2019], Gymnasium [Brockman et al., 2016, Todorov et al., 2012], and Weights & Biases [Biases, 2018]. Overall, we find that several of the code-level optimizations key to PPO reproducibility are superfluous for our method [Engstrom et al., 2020, Andrychowicz et al., 2021]. Particularly, we omit advantage normalization, value loss clipping [Schulman et al., 2017], gradient clipping, and modification of the default Adam [Kingma and Ba, 2014] epsilon parameter as they either do not lead to an appreciable difference in performance or have a slightly negative effect. However, we find that orthogonal weight initialization, learning rate annealing, reward scaling/clipping, and observation normalization/clipping remain having non-negligible positive effects on performance Engstrom et al. [2020], Andrychowicz et al. [2021]. In addition to adding dropout, weight decay regularization, and spectral normalization, we also look at model architecture modifications not present in the CleanRL implementation: layer width, number of hidden layers, layer activation, layer normalization Ba et al. [2016], and residual connections. We find that ReLU activation functions [Nair and Hinton, 2010], increasing layer width to 256, and a small dropout rate of 0.01-0.04 are beneficial. We find that network depth, and residual connections are benign overall. In contrast to recent findings in the context of offline data for off-policy reinforcement learning [Ball et al., 2023], we find that layer normalization — whether applied to the actor, the critic, or both — is detrimental to performance.

In Table 2, we present the hyperparameters used for the VSOP, VSPPO, RMPG, A3C, and PPO algorithms when trained on Gymnasium Mujoco environments. The table lists hyperparameters such as the number of timesteps, number of environments, learning rate, among others. Each algorithm may have a unique set of optimal hyperparameters. Please note that some hyperparameters such as ‘clip ϵ ’, ‘norm. adv.’, and ‘clip v-loss’ may not apply to all algorithms, as these are specific to certain policy optimization methods. The ‘width’ and ‘activation’ fields correspond to the architecture of the neural network used by the policy, and ‘weight decay’ and ‘dropout’ fields pertain to the regularization techniques applied during training. In general, tuning these hyperparameters properly is crucial to achieving optimal performance. Note that Adam optimization [Kingma and Ba, 2014] is used for all algorithms except for A3C where RMSProp [Hinton et al., 2012] is used.

All reported results are given as median values and standard error measurements over 10 random seeds.

B.2 Gymnax

We optimize hyperparameters of each algorithm across a variety of environments using a Bayesian optimization search strategy [Snoek et al., 2012]. Each algorithm is given a budget of 100 search steps and we use NVIDIA A100s. The hyperparameters we search over include learning rate, number of steps, number of environments, update epochs, number of minibatches, and the maximum gradient norm. We also search over the GAE λ parameter and hidden layer width for some environments. Each hyperparameter has a specific search space and transformation applied during the search. This is summarized in Table 3.

For the MinAtar environments, the hyperparameters are searched over a range, with the number of steps in [2, 8] (transformed to 2^x where x is the integer part of the sample), GAE λ in [0.0, 1.0] (rounded to the nearest multiple of 0.002), learning rate in [$1e - 4$, $1e - 3$] (rounded to the nearest multiple of 0.00005), update epochs in [1, 10] (rounded to the nearest integer), maximum gradient norm in [0.0, 5.0] (rounded to the nearest multiple of 0.1), number of minibatches in [0, 6] (transformed to 2^x), update epochs in [1, 10] (rounded to the nearest integer), and number of minibatches in [0, 7] (transformed to 2^x), and hidden layer width in [6, 10] (transformed to 2^x). The γ and number of environments are set to fixed values at 0.99 and 64 respectively.

For Mujoco-Brax, we do not search over the number of environments, or number of steps, instead setting them to fixed values at 0.99, 2048, and either 10 or 5 respectively. The other hyperparameters

Table 2: Hyper-parameters for PPO, VSOP, RMPG, A3C, and VSPPO algorithms across Gymnasium Mujoco environments

Parameter	Gymnasium Mujoco				
	VSOP	VSPPO	RMPG	A3C	PPO
timesteps	3e6	3e6	3e6	3e6	3e6
num. envs	1	1	1	1	1
num. steps	2048	2048	2048	5	2048
learning rate	3e-4	3e-4	3e-4	7e-4	3e-4
anneal lr	True	True	True	True	True
optim. ϵ .	1e-8	1e-8	1e-8	3e-6	1e-5
GAE γ	0.99	0.99	0.99	0.99	0.99
GAE λ	0.95	0.95	0.95	1.0	0.95
num. minibatch	32	32	32	1	32
update epochs	10	10	10	1	10
norm. adv.	False	False	False	False	True
clip ϵ	N/A	N/A	N/A	N/A	0.2
clip v-loss	False	False	False	False	True
ent. coef.	0.0	0.0	0.0	0.0	0.0
v-loss coef.	0.5	0.5	0.5	0.5	0.5
max grad. norm.	∞	∞	∞	0.5	0.5
norm. obs.	True	True	True	True	True
norm. reward	True	True	True	True	True
width	256	256	256	64	64
activation	relu	relu	relu	tanh	tanh
weight decay	2.4e-4	2.4e-4	2.4e-4	0.0	0.0
dropout	0.02	0.02	0.02	0.0	0.0

Hyperparameter	Range	Transformation	Transformed Range
num. envs	[2, 8]	2^x where x is int	{4, 8, 16, 32, 64, 128, 256}
num. steps	[2, 8]	2^x where x is int	{4, 8, 16, 32, 64, 128, 256}
λ	[0.0, 1.0]	round to multiple of 0.002	{0.0, 0.002, ..., 1.0}
learning rate	[1e-4, 1e-3]	round to multiple of 0.00005	{1e-4, 1.5e-5, ..., 1e-3}
max grad. norm.	[0.0, 5.0]	round to multiple of 0.1	{0.0, 0.1, ..., 5.0}
num. minibatch	[0, 6]	2^x where x is int	{1, 2, 4, 8, 16, 32, 64}
update epochs	[1, 10]	round to int	{1, 2, 3, ..., 10}
width	[6, 10]	2^x where x is int	{64, 128, 256, 512, 1024}

Table 3: Hyperparameter search space with transformations

are searched over the same ranges as the MinAtar environments. Further, to save time we only optimize over three environments: Humanoid, Hopper, and Reacher.

Finally, for Classic Control environments, we employ the same hyperparameter search as for MinAtar, except that we search over the number of environments in [2, 8] (transformed to 2^x where x is the integer part of the sample) and we do not search over the hidden layer width, instead setting it to a fixed value of 64.

This strategy allows us to thoroughly explore the hyperparameter space and find values that generalize well across a variety of different tasks. Further it allows us to fairly compare each algorithm. Table 4 reports the final hyper-parameter values for PPO, VSOP, and A3C.

All reported results are given as median values and standard error measurements over 5, 10, or 20 random seeds for MinAtar, Classic Control, and Mujoco-Brax respectively.

Table 4: Hyper-parameters for PPO, VSOP, and A3C algorithms across Gymnax environments

Parameter	MinAtar			Mujoco-Brax			Classic Control		
	PPO	VSOP	A3C	PPO	VSOP	A3C	PPO	VSOP	A3C
num. envs	64	64	64	2048	2048	2048	8	16	8
num. steps	32	64	8	10	10	5	8	64	4
GAE γ	0.99	0.99	0.99	0.99	0.99	0.99	0.99	0.99	0.99
GAE λ	0.9	0.9	0.9	0.982	0.926	0.97	0.54	0.58	0.13
learning rate	4e-4	6.5e-4	1e-3	3.5e-4	4e-4	7.5e-4	1e-3	8.5e-4	5.5e-4
max grad. norm.	2.1	2.4	0.7	4.7	2.1	4.1	3.4	1.9	3.8
num. minibatch	16	16	2	32	32	2	8	16	8
update epochs	5	10	1	2	2	1	3	8	1
clip ϵ	0.2	N/A	N/A	0.2	N/A	N/A	0.2	N/A	N/A
ent. coef.	0.01	0.01	0.01	0.0	0.0	0.0	0.01	0.01	0.01
activation	relu	relu	relu	relu	relu	relu	tanh	tanh	tanh
width	512	1024	128	512	512	64	64	64	64

C Additional Results

C.1 Comparing the effects of asynchronous parallelization and Thompson sampling

When tuning on the Mujoco-Brax environment, we found that the positive-effect of Thompson sampling on performance became diminished. In the Mujoco-Brax setting we used asynchronous parallelization with 2048 environments and just 10 steps per environment for 20480 steps per model update. Whereas in the Gymnasium setting we use just 1 environment and 2048 steps per update. Figure 6 summarizes an investigation to see if parallelization and/or update frequency mitigates the positive effects of Thompson sampling. This investigation is still on-going and we will leave it for follow up work. We do see, that Thompson sampling is necessary in the single environment setting: red-solid vs red-dashed lines. We also see that decreasing the update frequency and increasing parallelization seems to yield better results when no dropout is applied. This can be seen by comparing the smaller difference between solid and dashed purple lines (256 threads, 32768 steps per update) with the larger difference between solid and dashed orange lines (16 threads, 2048 steps per update). This is a progressive trend as we move through red, orange, yellow, green, blue, and purple. The trend is stable but more pronounced as we decrease the mini-batch size.

C.2 Spectral norm and Thompson sampling improve PPO

Interestingly, we see this same trend when applying spectral normalization and dropout to PPO. In Figure 7 we compare VSOP to the original PPO, and our own implementation that adds Thompson sampling and spectral normalization, VSPPO. In Figure 8 we compare how Thompson sampling and spectral norm effect PPO.

C.3 Classic Control

Figure 9 reports results for Classic Control.

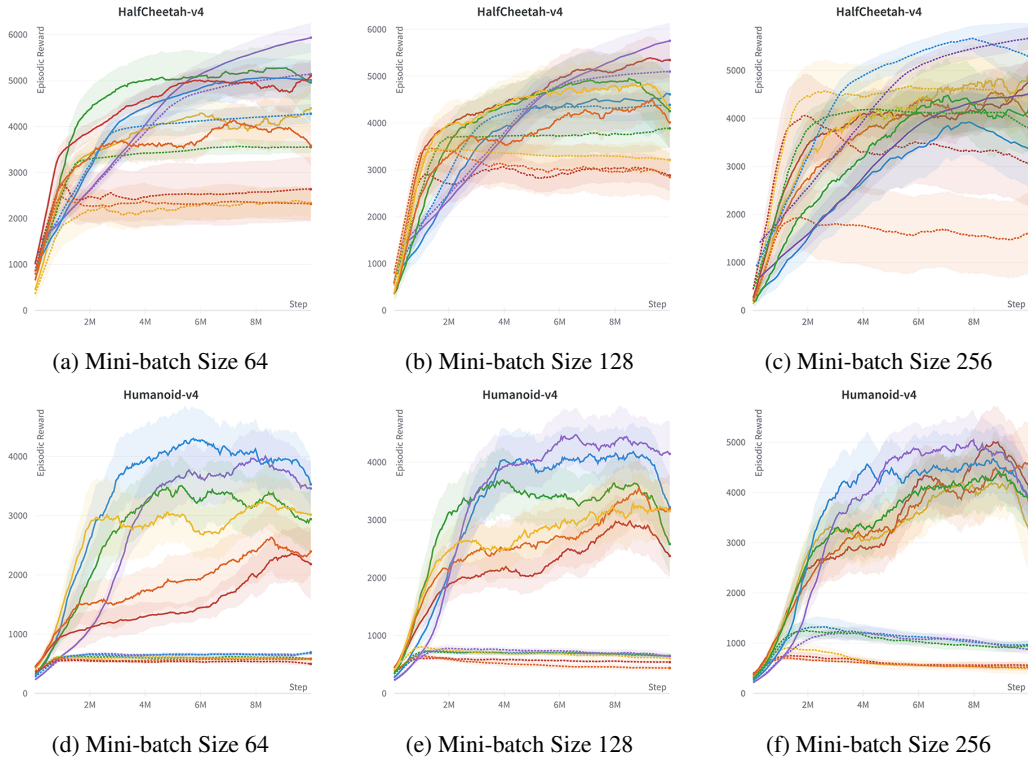


Figure 6: Investigating the connection between dropout and asynchronous parallelization. Top row, HalfCheetah-v4, Bottom row, Humanoid-v4. Solid lines, VSOP. Dashed lines, VSOP without dropout. Red: 1 thread, 2048 steps. Orange: 16 threads, 128 steps. Yellow: 32 threads, 128 steps. Green: 64 threads, 128 steps. Blue: 128 threads, 128 steps. Purple: 256 threads, 128 steps.

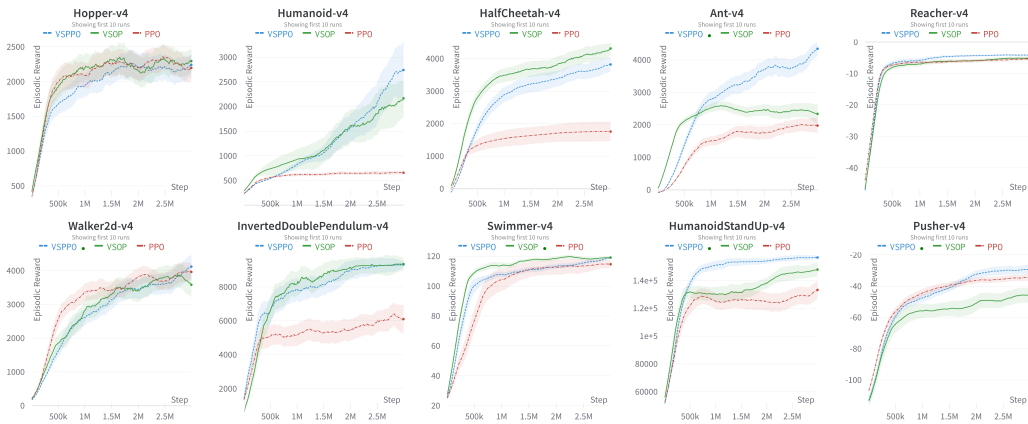


Figure 7: Mujoco continuous control benchmark comparison to PPO

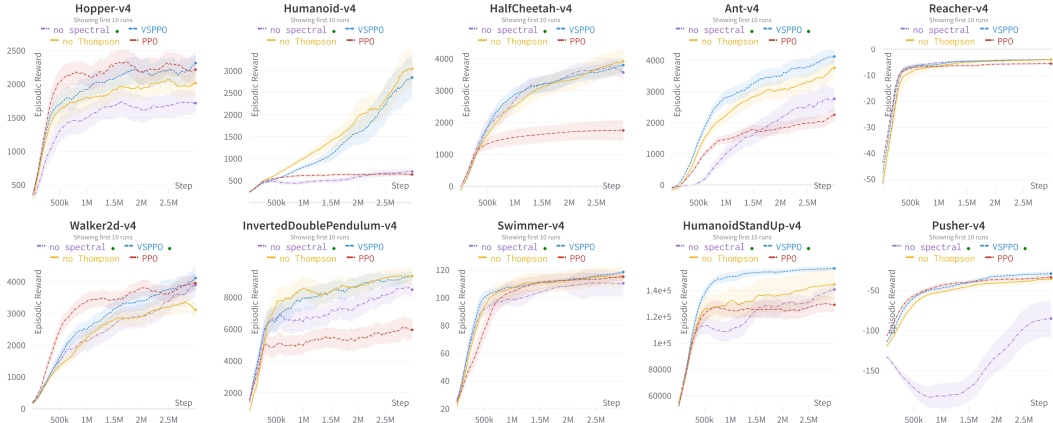


Figure 8: Mujoco continuous control benchmark examining the effect of Thompson sampling and spectral normalization on PPO.

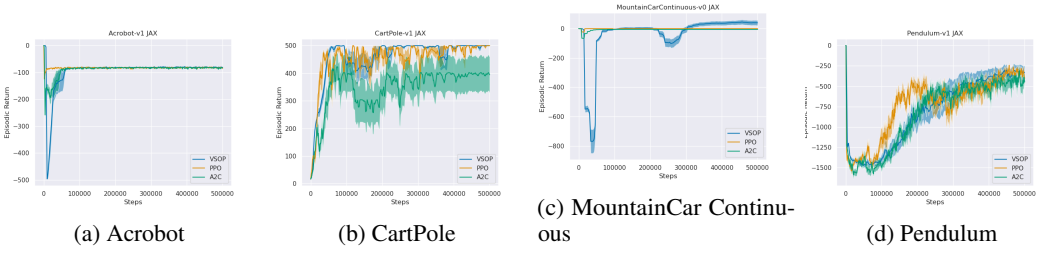


Figure 9: Classic Control Environments [Lange, 2022]. Here we show results for VSOP (Blue), PPO (Orange), and A3C (Green) for the Classic Control environments. We plot the mean episodic return and standard error measurement over 5 random seeds. Each method is tuned over several hyper-parameters using Bayesian Optimization [Snoek et al., 2012] with a budget of 100 search steps. Performance is effectively equal to PPO on Acrobot, CartPole, and Pendulum, but VSOP converges to a better solution on MountainCar Continuous. VSOP outperforms A3C on both MountainCar Continuous and CartPole.